Numer. Math. Theor. Meth. Appl.
doi: 10.4208/nmtma.2017.m1527

Vol. **10**, No. 3, pp. 562-596
August 2017

Analysis of Hexagonal Grid Finite Difference Methods for Anisotropic Laplacian Related Equations

Daniel Lee*

Department of Applied Mathematics, Tunghai University, Taichung 40704, Taiwan, Republic of China

Received 14 October 2015; Accepted (in revised version) 11 April 2016

Abstract. Hexagonal grids are valuable in two-dimensional applications involving Laplacian. The methods and analysis are investigated in current work in both linear and nonlinear problems related to anisotropic Laplacian. Ordinary and compact hexagonal grid finite difference methods are developed by elementary arguments, and then analyzed by perturbation for standard Laplacian. In the anisotropic case, analysis is done through reduction to the standard one by using Fourier vectors of mixed types. These hexagonal seven-point methods, with established theoretic stabilities and accuracies, are numerically confirmed in linear and semi-linear anisotropic Poisson problems, and can be applied also in time-dependent problems and in many applications in two-dimensional irregular domains.

AMS subject classifications: 65N06, 65N12, 65N22, 15A18, 15A63

Key words: Compact scheme, hexagonal grid method, matrix perturbation, fourier vectors.

1. Introduction

Hexagonal (Hex) grid methods are of interest in many research studies: [16] (direct method), [17] (has a formula without proof), [5] (seven-point method on rectangular grid with explicit form of eigen pairs), [27] (periodic boundary condition), [8–10] (numerical modeling in spherical coordinates), [7] (action potential in numerical heart modeling), [20] (showing advantages of Hex grids over commonly used square grids for use in atmospheric and ocean models). In the article [15], Hex grid FD methods are derived in a finite volume (FV) approach involving standard Laplacian, and used in the simulation of electrical wave phenomena propagated in two-dimensional reserved-C type cardiac tissue, exhibiting both linear and spiral waves more efficiently than similar computation carried on rectangular FVs. We note these cited works all used standard Laplacian and mostly on one configuration of regular hexagon.

*Corresponding author. *Email address:* danlee@thu.edu.tw (D. Lee)

 ©2017 Global-Science Press

https://doi.org/10.4208/nmtma.2017.m1527 Published online by Cambridge University Press

Aiming at two-dimensional applications involving anisotropic Laplacian (e.g., [21]), we extend in the current work the hexagonal seven-point methods to solving partial differential equations involving anisotropic Laplacian. Discretizations based on both ordinary and compact hexagonal seven-point methods are developed and analyzed. Also considered are the associated Hex grid discretizations with three-color iterative update [2,13,24]. The applications include linear and semilinear anisotropic Poisson equations.

In case of a configuration consisting of (subset of) Cartesian type regular hexagons, we denote by r the radius of a typical hexagon, h $(=\sqrt{3}r/2)$ the height, and d $(=2h)$ the *center-to-center* distance. At a typical center node, $P_0=(x_0,y_0)$, the six neighbor (center) nodes are

$$P_j=(x_j,y_j)=(x_0,y_0)+d(\cos\xi_j,\sin\xi_j),\quad \xi_j=\varphi+\frac{\pi}{6}+\frac{j\pi}{3},\quad j=1,\cdots,6. \tag{1.1}$$

Here the *phase angle*, φ, serves as the configurarion parameter. We focus on two particular instances : type I ($\varphi=0$) and type II ($\varphi=-\pi/6$). Hexagon centers in lattices of these two types are indexed as for an orthogonal Cartesian mesh as shown in Table 1, while the geometry and neighborhood of a general Hex FV in Table 2. We refer to Figs. 1(a), 1(b), 2(a), and 2(b) for visualization, and propose a three-color (Figs. 1(c) and 1(d)) algorithm in §4.2. In applications, a two-dimensional irregular domain may be approximated by a sequence of (not necessarily Cartesian) nets of hexagons. Actually, previous work in numerical modeling of electrocardiogram in a reversed C-type domain relies on this (Algorithm 1 in [15]).

Table 1: Lattices of type I and II regular hexagons.

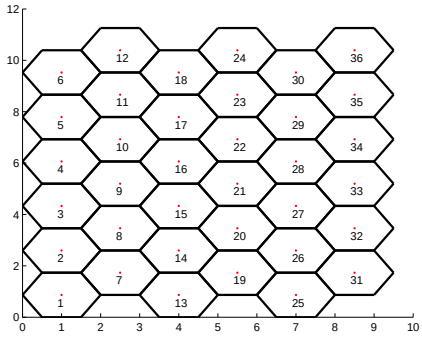
Phase angle	Type I, $\varphi=0$		Type II, $\varphi=-\pi/6$	
Center point	i^{even}	i^{odd}	j^{even}	j^{odd}
$cx(i,j)$	$(1.5i-0.5)r$		$2ih$	$(2i-1)h$
$cy(i,j)$	$2jh$	$(2j-1)h$	$(1.5j-0.5)r$	

Table 2: Local geometry at a hexagon : six vertices and six neighbor centers with indices periodically extended when appropriate.

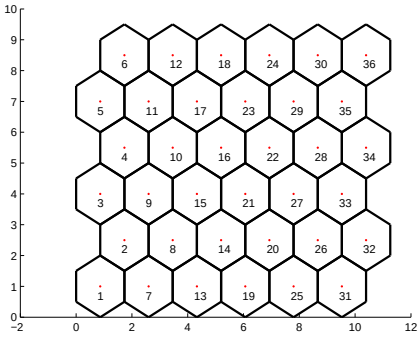
Phase angle	$\varphi\in\mathbb{R}$
Vertices	$V_k=\big(vx(*,k),vy(*,k)\big),\ k=1,2,\cdots,6$
$vx(*,k)$	$cx(*)+r\cos(\varphi+\frac{k\pi}{3})$
$vy(*,k)$	$cy(*)+r\sin(\varphi+\frac{k\pi}{3})$
Neighbor centers	$P_k=V_k+V_{k+1}-P_0,\qquad k=1,2,\cdots,6$

In analyzing the discrete anisotropic Laplacian, we note that, (i) spectral analysis of iterative methods on a net of hexagons seems not as easy as the analysis on square grids [12,25], because the set of finite trigonometric series is incomplete for the error analysis (even) on a single regular hexagon [18,19,26], and (ii) for Hex FVs of types I and II, con-

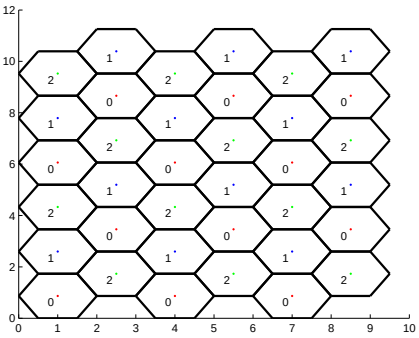
https://doi.org/10.4208/nmtma.2017.m1527 Published online by Cambridge University Press



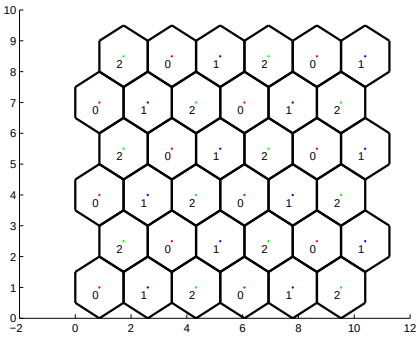
(a) Type I lattice in natural order by columns.



(b) Type II lattice in natural order by columns.



(c) Type I lattice in three colors and by columns.



(d) Type II lattice in three colors and by columns.

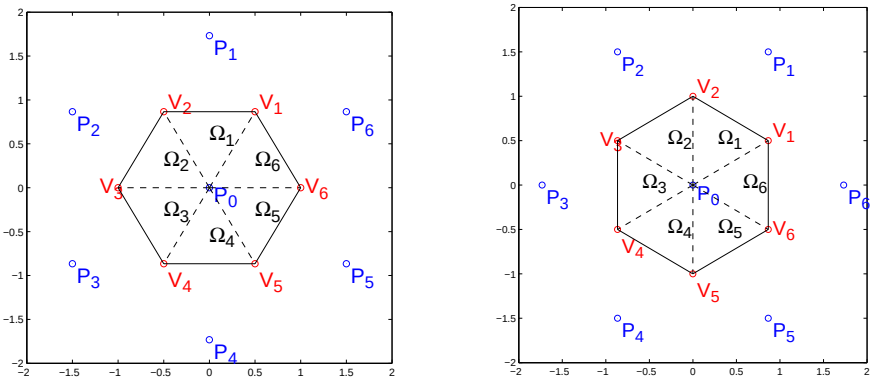
Figure 1: Lattice of hexagons in natural order with or without coloring.

vergence of schemes developed in the current work were analyzed using matrix properties by comparison and doubly confirmed via numerical investigation.

As for the remaining sections, we discuss Hex grid methods for solving anisotropic Poisson equation in §2, in which ordinary and compact seven-point discretizations of standard Laplacian are reviewed in §2.1 and extended on type I and II hexagons to anisotropic cases in §2.2 and §2.3 with stencil stability condition noted. Further theoretical discussion in terms of operators is given in §3.2, in which the perturbation analysis Eqs. (3.12) and (3.14) seems not applicable to all cases of the diffucivities ($D_1 \lesseqgtr D_2$). Success is reached in §3.3 in a detailed matrix analysis by a reduction to standard Laplacian together with usage of Fourier vectors of mixed types (Section 6). Nonlinear Poisson equations are analyzed in §3.4 and a result in global convergence is proved in §3.5. Precondtioning and a three-color algorithm for iterative methods are discussed in §4. Numerical experiments and discussions are given in §5, and conclusions drawn in the final section. In the appendix, §6, we use Fourier vectors of various mixed types to give detailed discussion for positive-definiteness of some relevant operators.

The main results are the hexagonal seven-point methods with error estimates for linear

https://doi.org/10.4208/nmtma.2017.m1527 Published online by Cambridge University Press



(a) Type I neighborhood. (b) Type II neighborhood.

Figure 2: Hexagonal FV neighborhood.

Poisson problems involving anisotropic Laplacian (Theorems 2.4 and 2.5), (lower) bound of spectrum of discrete hexagonal anisotropic Laplacian (Eq. (3.17)), stability and convergence of hexagonal methods on linear problems (Theorems 3.1, 3.2) and on nonlinear problems (Theorems 3.3), global convergence (Eq. (3.39)) in some semilinear test cases.

2. Hexagonal Schemes of Two-dimensional Anisotropic Laplacian

With positive constants D_1 and D_2, we consider the anisotropic Laplacian,

$$\boldsymbol{L_a}\, u := D_1 u_{xx} + D_2 u_{yy}, \tag{2.1}$$

which is approximated by hexagonal seven-point and orthogonal five-point schemes denoted by $\boldsymbol{L_{a7}}$ and $\boldsymbol{L_{a5}}$, respectively. In case of standard Laplacian ($D1 = D2 = 1$), these operators are denoted by $\boldsymbol{L_s}, \boldsymbol{L_{s7}}$ and $\boldsymbol{L_{s5}}$.

We discuss firstly solving linear anisotropic Poisson equation in the form,

$$\boldsymbol{L_a}\, u = f(x,y), \tag{2.2}$$

on a net of type I or II Hex FVs with phase angle $\varphi = 0$ or $-\pi/6$. The discretization of Eq. (2.2) at each Hex (center) node reads

$$\sum_{j=0}^{6} A_j u_{P_j} = \sum_{j=0}^{6} R_j (\boldsymbol{L_a} u)_{P_j}. \tag{2.3}$$

Here the stencils $\{A_j, R_j\}_{j=0}^{6}$ are 14 coefficients to be determined by one normalization constraint and several interpolation conditions on some properly chosen subset of monomials. These will be detailed in §2.3.

https://doi.org/10.4208/nmtma.2017.m1527 Published online by Cambridge University Press

2.1. Standard Laplacian ($D_1 = D_2 = 1$)

In the special case of solving standard Poisson equation, we mention the following results [15].

Theorem 2.1. (Second-order ordinary hexagonal seven-point (H7) scheme for standard Poisson equation.) *With an arbitrary phase angle, the expression*

$$\frac{1}{h^2}\left(\frac{1}{6}\sum_{j=1}^{6}u(P_j)-u(P_0)\right)=f(P_0)+\mathcal{O}(h^2), \tag{2.4}$$

is valid for $u \in \mathscr{C}^4$.

Theorem 2.2. (Fourth-order compact hexagonal seven-point (H7c) scheme for standard Poisson equation.) *With an arbitrary phase angle, the expression*

$$\frac{1}{h^2}\left(\frac{1}{6}\sum_{j=1}^{6}u(P_j)-u(P_0)\right)=\frac{3}{4}f(P_0)+\frac{1}{24}\sum_{j=1}^{6}f(P_j)+\mathcal{O}(h^4), \tag{2.5}$$

is valid for $u \in \mathscr{C}^6$.

Here the stencils are, $R = (1,0,0,0,0,0,0)$ and $(18,1,1,1,1,1,1)/24$ for H7 and H7c, respectively, and $A = (-6,1,1,1,1,1,1)/(6h^2)$ for both. In cases of using Hex I or II grid, the ordinary (H7) scheme is exact on 12 monomials $x^m y^n$ with $m+n \le 5$ except $\{x^4, y^4, x^2y^2\}$, while the compact (H7c) scheme is exact for at least 24 monomials $\{x^m y^n \mid 0 \le m,n,\ m+n \le 6\}$ except $\{x^6, y^6, x^4y^2, x^2y^4\}$.

2.2. Ordinary seven-point scheme for anisotropic Laplacian

In the current work, we extend the previous results to cases of general positive constants D_1 and D_2 on Hex grids of type I and II. When convenient and appropriate (for reading and compiling the mathematics at the same time), we will abuse the notations and use the following abbreviations.

Hex I.
$$\begin{aligned}\{P_j\}_{j=0}^6 &\equiv \{P,\ P_{_N},\ P_{_{NW}},\ P_{_{SW}},\ P_{_S},\ P_{_{SE}},\ P_{_{NE}}\},\\ \{A_j\}_{j=0}^6 &\equiv \{A_{_P},\ A_{_N},\ A_{_{NW}},\ A_{_{SW}},\ A_{_S},\ A_{_{SE}},\ A_{_{NE}}\}.\end{aligned} \tag{2.6a}$$

Hex II.
$$\begin{aligned}\{P_j\}_{j=0}^6 &\equiv \{P,\ P_{_{NE}},\ P_{_{NW}},\ P_{_W},\ P_{_{SW}},\ P_{_{SE}},\ P_{_E}\},\\ \{A_j\}_{j=0}^6 &\equiv \{A_{_P},\ A_{_{NE}},\ A_{_{NW}},\ A_{_W},\ A_{_{SW}},\ A_{_{SE}},\ A_{_E}\}.\end{aligned} \tag{2.6b}$$

Similarly with the primitive variable $\{u_{_{P_j}}\}_{j=0}^6$ and stencil $\{R_j\}_{j=0}^6$. The indexing and abbreviations are consistent with Table (2) and Figs. (2(a), 2(b)) .
We note results on a Hex II grid can be derived from that on a Hex I grid, and vice versa.

https://doi.org/10.4208/nmtma.2017.m1527 Published online by Cambridge University Press

Property 2.3. (Reflection principle.) *With the anisotropic Laplacian Eq.* (2.1) *defined on type I and II regular hexagons centered at the origin, the reflection with respect to the main diagonal in the xy-plane results in interchanging the types (phase angles) of hexagons and the two symbol lists,*

$$\{x, y, D_1, D_2, N, NW, SW, S, SE, NE\} \text{ and } \{y, x, D_2, D_1, E, SE, SW, W, NW, NE\}.$$

Theorem 2.4. (Second-order ordinary hexagonal seven-point (H7) scheme for anisotropic Laplacian.) *Consider cell-center FD discretization of Eq.* (2.2) *with $u \in \mathscr{C}^4$, the following two estimations are valid.*

(i) At Hex I grid,

$$\begin{aligned} &D_1 u_{xx} + D_2 u_{yy} \\ =&\frac{1}{6h^2}\Big(\frac{3D_2 - D_1}{2}(u_{_N} + u_{_S}) + D_1(u_{_{NE}} + u_{_{NW}} + u_{_{SE}} + u_{_{SW}}) - 3(D_1 + D_2)u_{_P}\Big) \\ &- \frac{h^2}{12}\Big(3D_1 u_{xxxx} + 6D_1 u_{xxyy} + (4D_2 - D_1)u_{yyyy}\Big) + \mathscr{O}(h^4). \end{aligned} \tag{2.7}$$

(ii) At Hex II grid,

$$\begin{aligned} &D_1 u_{xx} + D_2 u_{yy} \\ =&\frac{1}{6h^2}\Big(\frac{3D_1 - D_2}{2}(u_{_E} + u_{_W}) + D_2(u_{_{NE}} + u_{_{NW}} + u_{_{SE}} + u_{_{SW}}) - 3(D_1 + D_2)u_{_P}\Big) \\ &- \frac{h^2}{12}\Big((4D_1 - D_2)u_{xxxx} + 6D_2 u_{xxyy} + 3D_2 u_{yyyy}\Big) + \mathscr{O}(d^4). \end{aligned} \tag{2.8}$$

We derive the theorem using conventional FD notations. Since shifted monomials of the form $(x-x_0)^m(y-y_0)^n$ may offer slightly better numerical stability, we assume without loss of generality that

$$P_0 = (x_0, y_0) = (0, 0)$$

at a typical center node, and use standard monomials instead. The six neighbor nodes in Eq. (1.1) are

$$\text{(I)} \quad \begin{cases} (x_1, y_1) = -(x_4, y_4) = d(0,\ 1), \\ (x_2, y_2) = -(x_5, y_5) = d(\frac{-\sqrt{3}}{2}, \frac{1}{2}), \\ (x_3, y_3) = -(x_6, y_6) = d(\frac{-\sqrt{3}}{2}, \frac{-1}{2}), \end{cases} \tag{2.9a}$$

$$\text{(II)} \quad \begin{cases} (x_1, y_1) = -(x_4, y_4) = d(\frac{1}{2}, \frac{\sqrt{3}}{2}), \\ (x_2, y_2) = -(x_5, y_5) = d(\frac{-1}{2}, \frac{\sqrt{3}}{2}), \\ (x_3, y_3) = -(x_6, y_6) = d(-1,\ 0), \end{cases} \tag{2.9b}$$

at Hex grids of type I and II respectively.

https://doi.org/10.4208/nmtma.2017.m1527 Published online by Cambridge University Press

Proof of Theorem 2.4. A brief *formal* argument for a Hex I grid follows. Making use of the coordinates and assuming appropriate smoothness of the function u, truncated Taylor expansions yield,

$$\begin{aligned}
u_{NE}+u_{NW} &\approx 2u_P + 2\left(\frac{d}{2}u_y + \frac{d^2}{2}(\frac{3}{4}u_{xx}+\frac{1}{4}u_{yy}) + \frac{d^3}{6}(\frac{9}{8}u_{xxy}+\frac{1}{8}u_{xyy})\right.\\
&\qquad \left. + \frac{d^4}{24}(\frac{9}{16}u_{xxxx}+\frac{18}{16}u_{xxyy}+\frac{1}{16}u_{yyyy})\right),\\
u_{SE}+u_{SW} &\approx 2u_P + 2\left(-\frac{d}{2}u_y + \frac{d^2}{2}(\frac{3}{4}u_{xx}+\frac{1}{4}u_{yy}) + \frac{d^3}{6}(-\frac{9}{8}u_{xxy}-\frac{1}{8}u_{xyy})\right.\\
&\qquad \left. + \frac{d^4}{24}(\frac{9}{16}u_{xxxx}+\frac{18}{16}u_{xxyy}+\frac{1}{16}u_{yyyy})\right),
\end{aligned}$$

$$\begin{aligned}
&u_{NE}+u_{NW}+u_{SE}+u_{SW}-4u_P \qquad (2.10a)\\
&\qquad = d^2\left(\frac{3}{2}u_{xx}+\frac{1}{2}u_{yy}\right) + d^4\left(\frac{9}{96}u_{xxxx}+\frac{18}{96}u_{xxyy}+\frac{1}{96}u_{yyyy}\right)+\mathcal{O}(d^6),\\
&u_N+u_S-2u_P = d^2u_{yy}+\frac{d^4}{12}u_{yyyy}+\mathcal{O}(d^6). \qquad (2.10b)
\end{aligned}$$

Linear combination of the last two equations yields a second-order seven-point scheme for anisotropic Laplacian with an error estimate,

$$\begin{aligned}
&\frac{2D_1(u_{NE}+u_{NW}+u_{SE}+u_{SW})+(3D_2-D_1)(u_N+u_S)-6(D_1+D_2)u_P}{3d^2}\\
&= D_1u_{xx}+D_2u_{yy}+\frac{d^2}{48}\left(3D_1u_{xxxx}+6D_1u_{xxyy}+(4D_2-D_1)u_{yyyy}\right)+\mathcal{O}(d^4).
\end{aligned}$$

This ends the proof on a Hex I grid. Similar statements on a Hex II grid are implied by reflection (Property 2.3). □

Theorem 2.1 is thus generalized.

2.3. Compact seven-point scheme for Anisotropic Laplacian

Here we generalize Theorem 2.2.

Theorem 2.5. (Almost fourth-order compact hexagonal seven-point (H7c) scheme for anisotropic Laplacian.) *Consider the specific stencils,*

(i) at Hex I nodes,

$$\begin{aligned}
&\left(A_{NE}, A_{NW}, A_{SW}, A_{SE}, A_N, A_S, A_P\right)\\
&:=\frac{1}{12h^2}\left(2D_1,\ 2D_1,\ 2D_1,\ 2D_1,\ 3D_2-D_1,\ 3D_2-D_1,\ -6(D_1+D_2)\right), \qquad (2.11a)\\
&\left(R_{NE}, R_{NW}, R_{SW}, R_{SE}, R_N, R_S, R_P\right)\\
&:=\left(\frac{1}{24},\ \frac{1}{24},\ \frac{1}{24},\ \frac{1}{24},\ \frac{3-D_1/D_2}{48},\ \frac{3-D_1/D_2}{48},\ \frac{17+D_1/D_2}{24}\right), \qquad (2.11b)
\end{aligned}$$

https://doi.org/10.4208/nmtma.2017.m1527 Published online by Cambridge University Press

(ii) at Hex II nodes,

$$\begin{aligned}&\big(A_{NE},\,A_{NW},\,A_{SW},\,A_{SE},\,A_E,\,A_W,\,A_P\big)\\ :=&\frac{1}{12h^2}\Big(\,2D_2,\,2D_2,\,2D_2,\,2D_2,\,3D_1-D_2,\,3D_1-D_2,\,-6(D_1+D_2)\,\Big),\end{aligned}\tag{2.12a}$$

$$\begin{aligned}&\big(R_{NE},\,R_{NW},\,R_{SW},\,R_{SE},\,R_E,\,R_W,\,R_P\big)\\ :=&\Big(\,\frac{1}{24},\,\frac{1}{24},\,\frac{1}{24},\,\frac{1}{24},\,\frac{3-D_2/D_1}{48},\,\frac{3-D_2/D_1}{48},\,\frac{17+D_2/D_1}{24}\,\Big).\end{aligned}\tag{2.12b}$$

Then the following discretizations of Eq. (2.2) *with (local) error estimates are valid for* $u\in\mathscr{C}^6$.

$$\text{Hex I.}\quad \sum_{j=0}^{6}A_j u_{P_j}=\sum_{j=0}^{6}R_j(\boldsymbol{L_a}u)_{P_j}+\frac{(D_1-D_2)(D_1+3D_2)}{12D_2}u_{xxyy}h^2+\mathscr{O}(h^4),$$

$$\text{Hex II.}\quad \sum_{j=0}^{6}A_j u_{P_j}=\sum_{j=0}^{6}R_j(\boldsymbol{L_a}u)_{P_j}+\frac{(D_2-D_1)(D_2+3D_1)}{12D_1}u_{xxyy}h^2+\mathscr{O}(h^4).$$

We derive below the stencils and the leading error term by elementary argument. Using the coordinates (Eq. (2.9)), selected low degree monomials from the collection $\{u(x,y)=x^m y^n \mid 0\le m,n,\ m+n\le 6\}$ generate the interpolation conditions,

$$\sum_{j=0}^{6}A_j x_j^m y_j^n=\sum_{j=0}^{6}R_j(\boldsymbol{L_a}u)(x_j,y_j).\tag{2.13}$$

The above relations being scale-invariant, we set $R_0=1-\sum_1^6 R_j$ as normalization, and obtain $A_0=-\sum_1^6 A_j$ by the case $m=n=0$.

In view of the specific geometric symmetries (Figs. 2(a) and 2(b)) in the neighbors of a Hex node of type I or II, we assume the following symmetry in the stencils.

Assumption 2.1.

$$\begin{aligned}&\text{(Type I grid.)}\qquad &&A_N=A_S,\quad A_{NW}=A_{SW}=A_{SE}=A_{NE},\\ &&&R_N=R_S,\quad R_{NW}=R_{SW}=R_{SE}=R_{NE}.\\ &\text{(Type II grid.)}\qquad &&A_W=A_E,\quad A_{NW}=A_{SW}=A_{SE}=A_{NE},\\ &&&R_W=R_E,\quad R_{NW}=R_{SW}=R_{SE}=R_{NE}.\end{aligned}$$

Immediately obtained is the following.

Lemma 2.1. *With the assumed symmetry in both stencils, the aimed compact scheme on Hex I (or II) grid is exact on monomials of the form* $x^m y^n$*, with either* m *or* n *being odd.*

Proof. We focus on type I Hex grid. There remains four free coefficients, $\{A_N, A_{NE}, R_N, R_{NE}\}$. We use the fact that

$$\sum_{j=1}^{6}\sin^2\xi_j=\sum_{j=1}^{6}\cos^2\xi_j=3,\qquad \sum_{j=1}^{6}\sin^4\xi_j=\sum_{j=1}^{6}\cos^4\xi_j=\frac{9}{4}.$$

https://doi.org/10.4208/nmtma.2017.m1527 Published online by Cambridge University Press

The interpolation condition (Eq. (2.13)) with $(m,n)=(2,0)$ yields $A_2=A_3=A_5=A_6=2D_1/3d^2$, and then with $(m,n)=(0,2)$, $A_1=A_4=(3D_2-D_1)/3d^2$. We are thus led to reduced expressions, with $(m,n)=(4,0)$, that

$$12d^2D_1\sum_{j=1}^{6}R_j\cos^2\xi_j=\sum_{j=1}^{6}A_jx_j^4=\frac{3D_1}{2}d^2\,,$$

which yields $R_2=\frac{1}{24}$, and with $(m,n)=(0,4)$, that

$$12d^2D_2\sum_{j=1}^{6}R_j\sin^2\xi_j=\sum_{j=1}^{6}A_jy_j^4=\frac{4D_2-D_1}{2}d^2\,,$$

which in turn implies

$$R_1=R_4=\frac{3-D_1/D_2}{48}.$$

Similar results can be obtained directly on a Hex II grid, or by reflection (Property 2.3). The stencils Eqs. (2.11) and (2.12) are thus obtained with $d=2h$.

The compact scheme so constructed is *almost* fourth-order. It is exact at least on monomials with $0\le m,n,\ m+n\le 5$, except $(m,n)=(2,2)$, by the above construction and Lemma 2.1. The leading error term, up to a multiplicative factor

$$\frac{(\partial_x^2\partial_y^2)(u)}{(\partial_x^2\partial_y^2)(x^2y^2)}=\frac{u_{xxyy}}{4},$$

can be explicitly calculated using $u=x^2y^2$, such that,

$$\text{Hex I.}\quad \sum_{j=0}^{6}A_ju_{P_j}=\sum_{j=0}^{6}R_j(\boldsymbol{L_a}u)_{P_j}+\frac{(D_1-D_2)(D_1+3D_2)}{3D_2}h^2+\mathcal{O}(h^4),$$

$$\text{Hex II.}\quad \sum_{j=0}^{6}A_ju_{P_j}=\sum_{j=0}^{6}R_j(\boldsymbol{L_a}u)_{P_j}+\frac{(D_2-D_1)(D_2+3D_1)}{3D_1}h^2+\mathcal{O}(h^4).$$

Thus ends proving Theorem 2.5. □

Remark 2.1.

(1) Both H7 (Theorem 2.4) and H7c (Theorem 2.5) schemes yield the same A-stencil.

(2) Formulas of stencils A and R were obtained for general phase angles in [14] in a long discussion, by assuming only the central symmetry in stencil R ($R_{j+3}=R_j, j=1,2,3.$). The short proof of Theorem 2.5, as presented here for type I and II hexagonal grids, assumes that both stencils are symmetric wrt x- and y- axes (Assumption 2.1). We note there does exist instance of non-symmetric stencil of R [14].

https://doi.org/10.4208/nmtma.2017.m1527 Published online by Cambridge University Press

(3) (Stencil stability.) Positivity of all off-center weights Eqs. (2.7)–(2.8), or Eqs. (2.11)–(2.12) requires

$$\frac{1}{3} \le \frac{D_2}{D_1} \quad \text{at Hex I nodes}, \quad \text{and} \quad \frac{D_2}{D_1} \le 3 \quad \text{at Hex II nodes}. \tag{2.15}$$

We can always choose the phase angle of a Hex grid for a specific task without failing the above stencil stability.

We mention an important advantage of using a stable stencil in PDE discretization: local truncation errors decay in an iterative process (including a time march procedure).

3. Hexagonal grid methods for semilinear anisotropic Poisson equations

In this section, we discuss semilinear Poisson equation in the form

$$-D_1 u_{xx} - D_2 u_{yy} \equiv -\boldsymbol{L_a}\, u = f(u,x,y) \equiv f_1(x,y) - g(u), \tag{3.1}$$

which involves anisotropic Laplacian. Using analytic solution for error check and problem setup (the f-term in Eq. (3.1)), specific test problems in §5 include two anisotropic Poisson equations ($g = 0 = f_u$), a Helmholtz equation ($g = \lambda u$) and a semilinear equation ($g = u^2$).

We note the semilinear equation is usually approximated by successive linearization and solved iteratively. Rectangular five-point scheme is discussed next for comparison purpose at the matrices level.

3.1. Discrete quadrilateral five-point anisotropic Laplacian

The ordinary quadrilateral five-point (Q5) scheme on a Cartesian square grid with uniform meshsize $h_x (= h_y = h)$ is

$$\begin{aligned} &D_1 u_{xx} + D_2 u_{yy} \approx A_P^{(5)} u_P + A_W^{(5)} u_W + A_S^{(5)} u_S + A_N^{(5)} u_N + A_E^{(5)} u_E, \\ &\left(A_W^{(5)}, A_S^{(5)}, A_P^{(5)}, A_N^{(5)}, A_E^{(5)}\right) := \frac{1}{h_x^2}\left(\, D_1,\, D_2,\, -2(D_1+D_2),\, D_2,\, D_1 \,\right). \end{aligned}$$

Here the usage of the similar stencil notation ($A^{(5)}$) is restricted in this subsection only. Solving a linear algebraic system, $\boldsymbol{L_{a5}}\, u = -h_x^2 f$, then involves the (scaled) discrete five-point Laplacian. We express the corresponding linear operator on the discrete grid data space, in a form easy to compare later, as a block-tridiagonal matrix subscripted by size,

$$\boldsymbol{L_{a5}} = \text{B-trid}_{n_x}\left(\, \text{trid}_{n_y}(0, D_1, 0),\ \text{trid}_{n_y}(D_2, -2(D_1+D_2), D_2),\ \text{trid}_{n_y}(0, D_1, 0)\right), \tag{3.2}$$

in which each component block is in itself an ordinary *constant tridiagonal* (trid) matrix. Here the n_x-by-n_y nodes are ordered by columns.

https://doi.org/10.4208/nmtma.2017.m1527 Published online by Cambridge University Press

The complete eigen pairs are known in analytic form. For our purpose, we mention only the eigen values. Let

$$1 \le l \le n_x, \;\; 1 \le m \le n_y,$$

(i) With cell-center half-integral nodes and homogeneous Dirichlet B.C.,

$$\lambda_{l,m} = 4\left(D_1 \sin^2\left(\frac{l\pi/2}{n_x}\right) + D_2 \sin^2\left(\frac{m\pi/2}{n_y}\right)\right).$$

The maximum and minimum are, respectively,

$$\lambda_{n_x,n_y} = 4(D_1+D_2) \qquad \text{and} \qquad \lambda_{1,1} \approx \left(\frac{D_1\pi^2}{n_x^2} + \frac{D_2\pi^2}{n_y^2}\right). \tag{3.3}$$

(ii) With cell-center half-integral nodes and homogeneous Neumann B.C.,

$$\lambda_{l,m} = 4\left(D_1 \sin^2\left(\frac{(l-1)\pi/2}{n_x}\right) + D_2 \sin^2\left(\frac{(m-1)\pi/2}{n_y}\right)\right).$$

The maximal and some small values are

$$\lambda_{n_x,n_y} \approx 4(D_1+D_2) \quad \text{and} \quad \lambda_{1,1} = 0, \;\; \lambda_{2,1} \approx \frac{D_1\pi^2}{n_x^2}, \;\; \lambda_{1,2} \approx \frac{D_2\pi^2}{n_y^2}. \tag{3.4}$$

3.2. Discrete hexagonal ordinary seven-point (H7) anisotropic Laplacian

The ordinary discretization of Eq. (3.1) subject to Dirichlet boundary condition on an n_x-by-n_y Cartesian grid of Hex FVs yields a nonlinear algebraic system consisting of equations at all (interior) center nodes in the form (with the stencil specified in Eqs. (2.7) and (2.8);

$$\sum_{j=0}^{6} A_j u_{P_j} = -f_{P_j},$$

which defines the matrix representation at each linearization step in terms of general seven-point stencil,

$$\boldsymbol{L_{a7}}(I) := \text{B-trid}\left(\begin{bmatrix} 0 & \text{trid}(A_3,A_2,0) \\ 0 & 0 \end{bmatrix}, \begin{bmatrix} \text{trid}(A_4,A_0,A_1) & \text{trid}(A_5,A_6,0) \\ \text{trid}(0,A_3,A_2) & \text{trid}(A_4,A_0,A_1) \end{bmatrix}, \begin{bmatrix} 0 & 0 \\ \text{trid}(0,A_5,A_6) & 0 \end{bmatrix}\right),$$

up to the configuration in Figs. (1(a), 2(a)). Our discussion here focuses on type I hexagons.

With (central-)symmetric stencil ($A_j = A_{j+3}, \; j = 1,2,3$), the template reduces to the form

$$\boldsymbol{L_{a7}} = \text{B-trid}_{\frac{n_x}{2}}\left(\begin{bmatrix} 0 & M_2 \\ 0 & 0 \end{bmatrix}, \begin{bmatrix} M_1 & M_3 \\ M_3^T & M_1 \end{bmatrix}, \begin{bmatrix} 0 & 0 \\ M_2^T & 0 \end{bmatrix}\right),$$

https://doi.org/10.4208/nmtma.2017.m1527 Published online by Cambridge University Press

which is real symmetric and diagonally dominant. Strict diagonal dominance occurs at rows corresponding to the Dirichlet boundary condition. The negation of the matrix $\boldsymbol{L_{a7}}$ is therefore an *M-matrix*. These statements are valid for net of hexagons with every phase angle.

Further symmetry in Hex I case ($A_2 = A_3 = A_5 = A_6$) results in the simplification that

$$\boldsymbol{L_{a7}} = \text{B-trid}\left(\begin{bmatrix} 0 & A_2\,\text{trid}(1,1,0) & 0 \end{bmatrix}, \begin{bmatrix} \text{trid}(A_1,A_0,A_1) & A_2\,\text{trid}(1,1,0) \\ A_2\,\text{trid}(0,1,1) & \text{trid}(A_1,A_0,A_1) \end{bmatrix}, \begin{bmatrix} 0 & 0 \\ A_2\,\text{trid}(0,1,1) & 0 \end{bmatrix}\right),$$

or, in terms of solving $\boldsymbol{L_{a7}}\, u = -6h^2 f$ by scaling and using $d = 2h$, that

$$\boldsymbol{L_{a7}} = \text{B-trid}\left(\begin{bmatrix} 0 & D_1\,\text{trid}(1,1,0) & 0 \end{bmatrix}, \begin{bmatrix} \text{trid}(\frac{3D_2-D_1}{2}, -3D_1-3D_2, \frac{3D_2-D_1}{2}) & D_1\,\text{trid}(1,1,0) \\ D_1\,\text{trid}(0,1,1) & \text{trid}(\frac{3D_2-D_1}{2}, -3D_1-3D_2, \frac{3D_2-D_1}{2}) \end{bmatrix}, \begin{bmatrix} 0 & 0 \\ D_1\,\text{trid}(0,1,1) & 0 \end{bmatrix}\right). \tag{3.5}$$

We compare the two scaled algebraic systems,

$$\boldsymbol{L_{a5}}\, u = -h_x^2 f \qquad \text{and} \qquad \boldsymbol{L_{a7}}\, u = -6h^2 f, \tag{3.6}$$

at matrices level Eqs. (3.2) and (3.5) and observe that

$$\boldsymbol{L_{a7}} = \boldsymbol{L_{a5}} - (D_1 + D_2)\boldsymbol{I} + \boldsymbol{P_a}, \tag{3.7}$$

with the perturbation

$$\boldsymbol{P_a} := \text{B-trid}\left(\begin{bmatrix} 0 & \text{trid}(D_1,0,0) \\ 0 & 0 \end{bmatrix}, \begin{bmatrix} \frac{D_2-D_1}{2}\,\text{trid}(1,0,1) & \text{trid}(D_1,0,0) \\ \text{trid}(0,0,D_1) & \frac{D_2-D_1}{2}\,\text{trid}(1,0,1) \end{bmatrix}, \begin{bmatrix} 0 & 0 \\ \text{trid}(0,0,D_1) & 0 \end{bmatrix}\right). \tag{3.8}$$

In case of standard Laplacian ($D_1 = D_2 = 1$), the above relations simplify to

$$\boldsymbol{L_{s7}} = \boldsymbol{L_{s5}} - 2\boldsymbol{I} + \boldsymbol{P_s}, \tag{3.9}$$

with the perturbation

$$\boldsymbol{P_s} := \text{B-trid}_{\frac{n_x}{2}}\left(\begin{bmatrix} 0 & P_s \\ 0 & 0 \end{bmatrix}, \begin{bmatrix} 0 & P_s \\ P_s^T & 0 \end{bmatrix}, \begin{bmatrix} 0 & 0 \\ P_s^T & 0 \end{bmatrix}\right). \tag{3.10}$$

Here the component blocks of the perturbation are defined by

$$\begin{aligned} &\text{(Hex I)} \quad P_s = S_{n_y} := \text{trid}_{n_y}(1,0,0), \\ &\text{(Hex II)} \quad P_s = U_{n_y}, \qquad U_{n_y}(i,j) = \begin{cases} 1 & : \text{ if } j = i \pm 1, \text{ with odd } i, \\ 0 & : \text{ otherwise.} \end{cases} \end{aligned} \tag{3.11}$$

https://doi.org/10.4208/nmtma.2017.m1527 Published online by Cambridge University Press

For both type I and II lattices, $\|\boldsymbol{P_s}\| \leq 2$ in matrix row-sum, independent of the grid size. We conclude that the spectra of $(-\boldsymbol{L_{s5}})$ and $(-\boldsymbol{L_{s7}})$ satisfy

$$\max_{\sigma \in Spec_{-L_{s7}}} \min_{\mu \in Spec_{-L_{s5}+2I}} \{|\sigma - \mu|\} \leq \|\boldsymbol{P_s}\|_\infty \leq 2, \tag{3.12}$$

which together with Eq. (3.9) implies, by [3], that

$$\min Spec_{-L_{s7}} \geq \min Spec_{-L_{s5}} \approx \frac{\pi^2}{{n_x}^2} + \frac{\pi^2}{{n_y}^2}. \tag{3.13}$$

However, in the anisotropic case, it follows in matrix row-sum and independent of the meshsize (h_x in Q5 and h in H7) that,

$$\|\boldsymbol{P_a}\|_\infty \leq D_1 + D_2, \tag{3.14}$$

under an *additional* assumption that

$$D_2 \geq D_1. \tag{3.15}$$

We conclude, as a generalization of Eq. (3.12), that the spectra of $(-\boldsymbol{L_{a5}})$ and $(-\boldsymbol{L_{a7}})$ are *unitarily* close to each other [3],

$$\max_{\sigma \in Spec_{-L_{a7}}} \min_{\mu \in Spec_{-L_{a5}+(D_1+D_2)I}} \{|\sigma - \mu|\} \leq \|\boldsymbol{P_a}\|_\infty \leq D_1 + D_2, \tag{3.16}$$

such that, by Eqs. (3.3) and (3.7),

$$\min Spec_{-L_{a7}} \geq \min Spec_{-L_{a5}} \approx \frac{D_1\pi^2}{{n_x}^2} + \frac{D_2\pi^2}{{n_y}^2} = \mathcal{O}\left(\frac{1}{{n_x}^2} + \frac{1}{{n_y}^2}\right). \tag{3.17}$$

In case of a Hex II grid (ordered by columns), we just mention the discrete Laplacian

$$\boldsymbol{L_{a7}} = \text{B-trid}\left(\begin{bmatrix} 0 & \text{trid}(D_2, \frac{3D_1-D_2}{2}, D_2) \\ 0 & 0 \end{bmatrix}, \right.$$
$$\left. \begin{bmatrix} \text{trid}(D_2, -3D_1 - 3D_2, D_2) & \text{trid}(0, \frac{3D_1-D_2}{2}, 0) \\ \text{trid}(0, \frac{3D_1-D_2}{2}, 0) & \text{trid}(D_2, -3D_1 - 3D_2, D_2) \end{bmatrix}, \begin{bmatrix} 0 & 0 \\ \text{trid}(D_2, \frac{3D_1-D_2}{2}, D_2) & 0 \end{bmatrix}\right)$$

and the perturbation

$$\boldsymbol{P_a} := \text{B-trid}\left(\begin{bmatrix} 0 & \text{trid}(D_2, \frac{D_1-D_2}{2}, D_2) \\ 0 & 0 \end{bmatrix}, \right.$$
$$\left. \begin{bmatrix} 0 & \text{trid}(0, \frac{D_1-D_2}{2}, 0) \\ \text{trid}(0, \frac{D_1-D_2}{2}, 0) & 0 \end{bmatrix}, \begin{bmatrix} 0 & 0 \\ 0 & \text{trid}(D_2, \frac{D_1-D_2}{2}, D_2) \end{bmatrix}\right).$$

It is similar in this case, $\|\boldsymbol{P_a}\|_\infty \leq D_1 + D_2$, provided that $D_1 > D_2$.

https://doi.org/10.4208/nmtma.2017.m1527 Published online by Cambridge University Press

Remark 3.1.

(1) The same A-stencil (Eqs. (2.7), (2.8), (2.11) and (2.12)) are retained in both H7 and H7c schemes. The matrix analysis here applies to H7c as well, with the R_j-terms kept on the RHS as source term of Eq. (2.3).

(2) The perturbation analysis in the current subsection seems difficult to cover either the case that $D_2 < D_1$ on a Hex I grid or $D_1 < D_2$ on a Hex II grid. For such, in the next subsection we take a different view which relates the anisotropic Laplacian to standard Laplacian.

3.3. Discrete type I hexagonal compact seven-point (H7c) anisotropic Laplacian

General cases of Eq. (3.14) are discussed here. The compact discretization of Eq. (3.1) subject to Dirichlet boundary condition on an n_x-by-n_y Cartesian grid of Hex FVs yields a nonlinear algebraic system consisting of equations at all (interior) center nodes in the form (using the stencil aliased in Eq. (2.6a)) that

$$-\sum_{j=0}^{6} A_j u_{P_j} = \sum_{j=0}^{6} R_j f_{P_j},$$

which defines the matrix representation at each linearization step using H7c stencils (Theorem 2.5). To recast the equation, we define the (scaled) *total incidence* matrix

$$\boldsymbol{E_a} := \sum_{j=1}^{6} h^2 A_j \boldsymbol{E_j} = \sum_{j=1}^{3} h^2 A_j (\boldsymbol{E_j} + \boldsymbol{E_{j+3}})$$

in terms of six *primitive* incidence matrices which are abbreviated (in the order stated in Eq. (2.6a)) as

$$\begin{aligned} &\text{(Hex I)} && \{\boldsymbol{E_j}\}_{j=1}^{6} \equiv \{\boldsymbol{E_N}, \boldsymbol{E_{NW}}, \boldsymbol{E_{SW}}, \boldsymbol{E_S}, \boldsymbol{E_{SE}}, \boldsymbol{E_{NE}}\}, \\ &\text{(Hex II)} && \{\boldsymbol{E_j}\}_{j=1}^{6} \equiv \{\boldsymbol{E_{NE}}, \boldsymbol{E_{NW}}, \boldsymbol{E_W}, \boldsymbol{E_{SW}}, \boldsymbol{E_{SE}}, \boldsymbol{E_E}\}. \end{aligned} \tag{3.18}$$

Here, for example, with indices p and q running through all (interior) center nodes,

$$\boldsymbol{E_{NW}}(p,q) = \begin{cases} 1, & \text{if the q-th node is the NW-neighbor to the p-th node,} \\ 0, & \text{otherwise.} \end{cases}$$

Notice that

$$\boldsymbol{E_{j+3}} = \boldsymbol{E_j^T}$$

and therefore $(\boldsymbol{E_j} + \boldsymbol{E_{j+3}})$ are symmetric with $j = 1, 2, 3$.

We now recast the (probably nonlinear) discrete system as

$$\boldsymbol{Q_{2a}} u = h^2 \boldsymbol{Q_{1a}} f, \quad u = h^2 \boldsymbol{K_a} f. \tag{3.19}$$

https://doi.org/10.4208/nmtma.2017.m1527 Published online by Cambridge University Press

The defining relations are

$$\boldsymbol{Q_{2a}} = -h^2 A_0 \boldsymbol{I} - \boldsymbol{E_a} = \frac{D_1 + D_2}{2}\boldsymbol{I} - \sum_{j=1}^{6} h^2 A_j \boldsymbol{E_j}, \tag{3.20a}$$

$$\boldsymbol{Q_{1a}} = R_0 \boldsymbol{I} + \sum_{j=1}^{6} R_j \boldsymbol{E_j} = \frac{17 + D_1/D_2}{24}\boldsymbol{I} + \sum_{j=1}^{6} R_j \boldsymbol{E_j}, \tag{3.20b}$$

$$\boldsymbol{K_a} = \boldsymbol{Q_{2a}}^{-1}\boldsymbol{Q_{1a}}. \tag{3.20c}$$

We note some qualitative properties.

1. As an averaging operator with symmetric positive weights, $\boldsymbol{Q_{1a}}$ is symmetric and therefore positive-definite. In case of an ordinary H7 method, $\boldsymbol{Q_{1a}}$ is simply the $identity$.
2. The (total) incidence operator ($\boldsymbol{E_a}$) is real symmetric and therefore diagonalizable.
3. The operator $\boldsymbol{Q_{2a}}$ is symmetric with positive entities in the main diagonal and negative (or zero) entities off the diagonal. It is weakly diagonally dominant with strict dominance at all next-to-boundary interior nodes. Therefore, $\boldsymbol{Q_{2a}}$ is symmetric and positive-definite, and is an M-matrix and inverse-positive [2, 4, 11].
4. Being well-defined, $\boldsymbol{K_a}$ is symmetric and positive-definite.
5. The pair $\boldsymbol{Q_{2a}}$ and $\boldsymbol{E_a}$ commute and have same (complete) basis set.
6. In the anisotropic case ($D_1 \neq D_2$) and with H7c scheme, $\boldsymbol{Q_{1a}}$ and $\boldsymbol{E_a}$ do not commute, because $\boldsymbol{E_a}$ and the incidence components of $\boldsymbol{Q_{1a}}$ are not proportional. That is, $\{A_j\}_{j=1}^6$ and $\{R_j\}_{j=1}^6$ are not parallel.
7. In case of standard Laplacian ($D_1 = D_2$), all the symmetric matrices $\boldsymbol{E}(\equiv \boldsymbol{E_a})$, $\boldsymbol{Q_{2s}}$, $\boldsymbol{Q_{1s}}$ and $\boldsymbol{K_s}$ commute pairwisely and have same eigen basis set.

To prove Eq. (3.14) without assuming Eq. (3.15), we observe two expressions,

$$(D_2 \geq D_1) \qquad -D_1 u_{xx} - D_2 u_{yy} = \big(-D_1(u_{xx} + u_{yy})\big) + \big(-(D_2 - D_1)u_{yy}\big), \tag{3.21a}$$

$$(D_1 \geq D_2) \qquad -D_1 u_{xx} - D_2 u_{yy} = \big(-D_2(u_{xx} + u_{yy})\big) + \big(-(D_1 - D_2)u_{xx}\big). \tag{3.21b}$$

Under the assumptions as indicated, both the above express the negative anisotropic Laplacian as the sum of a positive and a non-negative (differential) operators when properly interpreted. This guides manipulations which result in discrete analogues.

Theorem 3.1. *Let the stencil stability condition Eq.* (2.15) *be satisfied on a Hex I grid. Then, one of the alternatives*

$$(\text{if } D_2 \geq D_1,) \qquad \boldsymbol{Q_{2a}} \equiv -\boldsymbol{L_{a7}} = D_1 \boldsymbol{Q_{2s}} + \frac{3(D_2 - D_1)}{2}(2\boldsymbol{I} - \boldsymbol{E}_N - \boldsymbol{E}_s), \tag{3.22a}$$

$$(\text{if } D_1 \geq D_2,) \qquad \boldsymbol{Q_{2a}} \equiv -\boldsymbol{L_{a7}} = D_2 \boldsymbol{Q_{2s}} + \frac{D_1 - D_2}{2}\boldsymbol{Q_3}, \tag{3.22b}$$

https://doi.org/10.4208/nmtma.2017.m1527 Published online by Cambridge University Press

implies that the discrete seven-point negative Laplacian is a positive operator. Here

$$(-12h^2\cdot\partial_x^2\approx)\,\boldsymbol{Q_3}:=6\boldsymbol{I}+\boldsymbol{E}_N+\boldsymbol{E}_S-2\boldsymbol{E}_{NE}-2\boldsymbol{E}_{SW}-2\boldsymbol{E}_{NW}-2\boldsymbol{E}_{SE}. \tag{3.23}$$

Proof. By definition of the A-stencil (Eq. (2.11)),

$$\begin{aligned}
&-6h^2\boldsymbol{L}_{a7}\\
=&-\big(D_1,D_1,D_1,D_1,\frac{3D_2-D_1}{2},\frac{3D_2-D_1}{2},-3D_1-3D_2\big)\cdot\big(\boldsymbol{E}_{NE},\boldsymbol{E}_{NW},\boldsymbol{E}_{SW},\boldsymbol{E}_{SE},\boldsymbol{E}_N,\boldsymbol{E}_S,\boldsymbol{I}\big)^T\\
=&D_1\big(-\boldsymbol{E}_{NE}-\boldsymbol{E}_{NW}-\boldsymbol{E}_{SW}-\boldsymbol{E}_{SE}-\boldsymbol{E}_N-\boldsymbol{E}_S+6\boldsymbol{I}\big)+\frac{3(D_2-D_1)}{2}\big(-\boldsymbol{E}_N-\boldsymbol{E}_S+2\boldsymbol{I}\big).
\end{aligned}$$

The matrix $(2\boldsymbol{I}-\boldsymbol{E}_N-\boldsymbol{E}_S)$ is (tridiagonal and) S.P.D. by M-matrix theory. We omit explicit expressions of its eigen pairs. This yields the first alternative. For the second one, notice that

$$\begin{aligned}
-6h^2\boldsymbol{L}_{a7}=&D_2\big(-\boldsymbol{E}_{NE}-\boldsymbol{E}_{NW}-\boldsymbol{E}_{SW}-\boldsymbol{E}_{SE}-\boldsymbol{E}_N-\boldsymbol{E}_S+6\boldsymbol{I}\big)\\
&+\frac{D_1-D_2}{2}\big(-2,-2,-2,-2,1,1,6\big)\cdot\big(\boldsymbol{E}_{NE},\boldsymbol{E}_{NW},\boldsymbol{E}_{SW},\boldsymbol{E}_{SE},\boldsymbol{E}_N,\boldsymbol{E}_S,\boldsymbol{I}\big)^T.
\end{aligned}$$

The fact that $\boldsymbol{Q_3}$ is positive-definite is rigorously proved in Theorem A.2. Actually, $\boldsymbol{Q_3}$ being positive semidefinite is sufficient. We give here an informal argument. To this end, a linear combination of Eqs. (2.10a) and (2.10b) yields

$$\begin{aligned}
&6u_P+u_N+u_S-2u_{NE}-2u_{NW}-2u_{SW}-2u_{SE}\\
=&-3d^2u_{xx}-\frac{3d^4}{16}(u_{xxxx}+2u_{xxyy}+u_{yyyy})+\frac{d^4}{4}u_{yyyy}+\mathcal{O}(d^6)\\
=&-3d^2u_{xx}+\mathcal{O}(d^4).
\end{aligned}$$

This ends the proof. □

An immediate consequence follows.

Corollary 3.1. *Assume the stencil stability condition Eq.* (2.15) *is satisfied on a Hex I grid.*

$$\text{If } D_2\ge D_1,\qquad \text{then } \boldsymbol{Q_{2a}}\ge D_1\boldsymbol{Q_{2s}}. \tag{3.24a}$$

$$\text{If } D_1\ge D_2,\qquad \text{then } \boldsymbol{Q_{2a}}\ge D_2\boldsymbol{Q_{2s}}. \tag{3.24b}$$

We note some quantitative properties.

1. Bounds of spectrum of the positively-weighted averaging operator are available by Gershgorin's theory,

$$\frac{5+\frac{D_1}{D_2}}{12}=R_0-\sum_{j=1}^{6}R_j\le Spec_{\mathbf{Q}_{1a}}\le R_0+\sum_{j=1}^{6}R_j=1. \tag{3.25}$$

https://doi.org/10.4208/nmtma.2017.m1527 Published online by Cambridge University Press

2. Similarly, an upper bound of the discrete negative anisotropic Laplacian can be derived,

$$Spec_{\mathbf{Q}_{2a}} \le |h^2 A_0| + \sum_{j=1}^{6} |h^2 A_j| = D_1 + D_2. \tag{3.26}$$

We appeal to Corollary 3.1 and Eq. (3.3) for a lower bound.

$$\text{If } D_2 \ge D_1, \quad \text{then } D_1 2\pi^2 h^2 \approx D_1 \min Spec_{\mathbf{Q}_{2s}} \le \min Spec_{\mathbf{Q}_{2a}}. \tag{3.27a}$$

$$\text{If } D_1 \ge D_2, \quad \text{then } D_2 2\pi^2 h^2 \approx D_2 \min Spec_{\mathbf{Q}_{2s}} \le \min Spec_{\mathbf{Q}_{2a}}. \tag{3.27b}$$

3. With $D_2 \ge D_1$, the lower bound above is not as sharp as already obtained in Eq. (3.17), the latter implies

$$\begin{aligned} \frac{(5 + D_1/D_2)/12}{D_1 + D_2} h^2 &\le h^2 \frac{\min Spec_{\mathbf{Q}_{1a}}}{\max Spec_{\mathbf{Q}_{2a}}} \\ &\le h^2 Spec_{\mathbf{K}_a} \le h^2 \frac{\max Spec_{\mathbf{Q}_{1a}}}{\min Spec_{\mathbf{Q}_{2a}}} \le \frac{1}{(D_1 + D_2)\pi^2}. \end{aligned} \tag{3.28}$$

4. If $D_1 \ge D_2$, the first part of the above Equation still holds, while the non-negativity of operator $\mathbf{Q_3}$ yields

$$h^2 Spec_{\mathbf{K}_a} \le h^2 \frac{\max Spec_{\mathbf{Q}_{1a}}}{\min Spec_{\mathbf{Q}_{2a}}} \le \frac{1}{2D_2\pi^2}. \tag{3.29}$$

Although not an optimal upper bound as would be expected, it suffices for our purpose as Remark 3.1 (item (2)) is concerned.

In summary, we have

Theorem 3.2. (Linear stability of H7 and H7c on anisotropic Poisson problems.) *Let the stencil stability condition Eq.* (2.15) *be satisfied in solving anisotropic Poisson problem (Eq.* (3.1) *with $f_u = 0$) using hexagonal ordinary or compact seven-point method, then the discrete system Eq.* (3.19) *can be uniquely and stably solved as the grid refines.*

Proof. As $h \to 0$, the net of discretization operators are consistent (as being of second or fourth-order) and uniformly bounded from above by Eqs. (3.28) and (3.29). Convergence is therefore guaranteed [1]. □

A general nonlinear result is true as shown next.

3.4. Convergence of Hex schemes in solving nonlinear Poisson equation

For simplicity of the notations, we assume here and in the next subsection that $D_1 = D_2 = 1$.

https://doi.org/10.4208/nmtma.2017.m1527 Published online by Cambridge University Press

Theorem 3.3. (Nonlinear stability of H7c scheme.) *In solving the nonlinear Poisson problem*

$$-u_{xx} - u_{yy} = f(u, x, y), \tag{3.30}$$

if $\|f\|_\infty$ *and* $\|f_u\|_\infty$ *are finite on a bounded region in the* xy*-plane with* $\|f_u\|_\infty < 2\pi^2$*, then the problem*

$$\boldsymbol{Q_{2s}} u = h^2 \boldsymbol{Q_{1s}} f, \qquad u = h^2 \boldsymbol{K_s} f \tag{3.31}$$

with

$$\boldsymbol{Q_{2s}} := \boldsymbol{I} - \frac{1}{6}\boldsymbol{E}, \qquad \boldsymbol{Q_{1s}} := \frac{3}{4}\boldsymbol{I} + \frac{1}{24}\boldsymbol{E}, \qquad \boldsymbol{K_s} := \boldsymbol{Q_{2s}}^{-1}\boldsymbol{Q_{1s}}, \tag{3.32}$$

can be uniquely and stably solved as the grid refines.

Proof. With superscripts denoting for iteration counts and $u^{(0)}$ an initial vector, application of SS procedure in a constructive approach to solving the nonlinear Poisson Eq. (3.30) discretized by H7c scheme (Eqs. (3.31)) yields

$$u^{(k)} := \boldsymbol{\Phi} u^{(k-1)} := \frac{1}{6}\boldsymbol{E} u^{(k-1)} + h^2 \boldsymbol{Q_{1s}} f(u^{(k-1)}, x, y), \qquad k = 1, 2, 3, \ldots . \tag{3.33}$$

We can choose h as small as to make valid the following estimate of the contraction rate

$$\begin{aligned} \|D\boldsymbol{\Phi}\| &\le \frac{1}{6}\|\boldsymbol{E}\| + h^2 \|\boldsymbol{Q_{1s}}\| \cdot \|f_u\|_\infty \le 1 - \sigma_{sm} + h^2 \left(1 - \frac{\sigma_{sm}}{4}\right) \|f_u\|_\infty \\ &\lesssim 1 - (2\pi^2 - \|f_u\|_\infty) h^2 - \frac{\pi^2}{2}\|f_u\|_\infty h^4, \end{aligned} \tag{3.34}$$

in which

$$\sigma_{sm} := \min Spec_{\boldsymbol{Q_{2s}}} \approx 2\pi^2 h^2 > 0.$$

Convergence is therefore established. □

The argument is similar in case of using H7 scheme instead, with the averaging operator $\boldsymbol{Q_{1s}}$ replaced by the *identity* and the term $(1 - \sigma_{sm}/4)$ replaced by 1. That is,

$$u^{(k)} := \boldsymbol{\Phi} u^{(k-1)} := \frac{1}{6}\boldsymbol{E} u^{(k-1)} + h^2 f\left(u^{(k-1)}, x, y\right), \quad k = 1, 2, \cdots, \tag{3.35a}$$

$$\|D\boldsymbol{\Phi}\| \le \frac{1}{6}\|\boldsymbol{E}\| + h^2 \|f_u\|_\infty \le 1 - \sigma_{sm} + h^2 \|f_u\|_\infty \approx 1 - (2\pi^2 - \|f_u\|_\infty) h^2. \tag{3.35b}$$

Remark 3.2. Although both the estimates Eqs. (3.34) and (3.35b) are pessimistic, the above discussion suggests that compared with ordinary seven-point scheme, the compact scheme (i) admits relatively coarser grid resolutions by smaller contraction rate, and (ii) converges faster in iteration count by smaller operator norm.

https://doi.org/10.4208/nmtma.2017.m1527 Published online by Cambridge University Press

3.5. Global convergence in test problems

In general, (only) local convergence in Eqs. (3.33) and (3.35a) are valid in (restricted) regions with small $\|f_u\|_\infty$ for a contraction by Eqs. (3.34) and (3.35b). However, global convergence are obtained in our test problems in §5, for which (with $D_1 = D_2 = 1$ in Eq. (3.1))

$$-u_{xx} - u_{yy} = f(u,x,y) \equiv f_1(x,y) - u * g_1(u) \tag{3.36}$$

with $g_1(u) = 0, \lambda(>0)$, or u. So that discretization of the $u * g_1(u)$ term, when moved to the left-hand side of the discrete system, yields positive operator (same as the negative Laplacian), and therefore

$$\|D\boldsymbol{\Phi}\| \le 1 - \sigma_{sm} \lesssim 1 - 2\pi^2 h^2 = 1 - \mathcal{O}(h^2)$$

holds with both H7c and H7 schemes. In some detail, the discretizations in our test problems,

$$\left(\boldsymbol{I} - \frac{1}{6}\boldsymbol{E}\right) u + h^2 \boldsymbol{Q_{1s}}(u * g_1(u)) = h^2 \boldsymbol{Q_{1s}} f_1$$

suggests iterations (in terms of *element-wise* multiplications involving the weighted average)

$$\left(\boldsymbol{I} + h^2 \boldsymbol{Q_{1s}} \,.*\, g_1(u^{(k-1)})\right) u^{(k)} = \frac{1}{6}\boldsymbol{E} u^{(k-1)} + h^2 \boldsymbol{Q_{1s}} f_1, \tag{3.37}$$

namely,

$$u^{(k)} := \boldsymbol{\Phi}_k u^{(k-1)} \equiv (\boldsymbol{I} + h^2 \boldsymbol{Q_{1s}} \,.*\, g_1(u^{(k-1)}))^{-1} \left(\frac{1}{6}\boldsymbol{E} u^{(k-1)} + h^2 \boldsymbol{Q_{1s}} f_1\right), \tag{3.38}$$

with

$$\|D\boldsymbol{\Phi}_k\| \le \frac{1}{1 - h^2 \|\boldsymbol{Q_{1s}}\| \cdot \|g_1\|_\infty} \cdot \|\frac{1}{6}\boldsymbol{E}\| \le \|\frac{1}{6}\boldsymbol{E}\| = 1 - \sigma_{sm} = 1 - \mathcal{O}(h^2). \tag{3.39}$$

We note the primitive variables are usually non-dimensionalized close to unit magnitude in practical applications.

We refer to [6] for solving a general (dense) Block Toeplitz matrix consisting of Toeplitz Blocks (BTTB) using FFT.

4. Computational Issues

Issues in acceleration of convergence is discussed here. We assume $D_1 = D_2 = 1$ for ease of notations, and consider solving the scaled discrete hexagonal nonlinear Poisson equation,

$$-\boldsymbol{L_{s7}}\, u = 6h^2 f(u,x,y).$$

https://doi.org/10.4208/nmtma.2017.m1527 Published online by Cambridge University Press

4.1. Preconditioning Hex schemes in solving nonlinear standard Poisson

Several variants of matrix splitting exist [2, 24]. Convergence of Jacobi (diagonal) preconditioner is discussed in Eqs. (3.33)–(3.35b) and (3.39). We mention below a block-Jacobi type preconditioner.

At each grid resolution (with fixed h), we consider the matrix splitting on a Hex I grid

$$-\boldsymbol{L}_{s7} = \big(6\boldsymbol{I} - \boldsymbol{E}_N - \boldsymbol{E}_s\big) - \big(\boldsymbol{E}_{NE} + \boldsymbol{E}_{NW} + \boldsymbol{E}_{SE} + \boldsymbol{E}_{SW}\big).$$

The implied preconditioner is actually a direct sum. It is a block-diagonal matrix with identical square blocks,

$$\big(6\boldsymbol{I} - \boldsymbol{E}_N - \boldsymbol{E}_s\big) = \text{B-diag}_{n_x}\big(\text{trid}_{n_y}(-1, 6, -1)\big). \tag{4.1}$$

In the nonlinear case,

$$-\boldsymbol{L}_{s7}\, u^{(k)} = 6h^2 f\left(u^{(k-1)}, x, y\right),$$

the SS procedure at each linearized stage,

$$\big(6\boldsymbol{I} - \boldsymbol{E}_N - \boldsymbol{E}_s\big)u^{(k)} = \big(\boldsymbol{E}_{NE} + \boldsymbol{E}_{NW} + \boldsymbol{E}_{SE} + \boldsymbol{E}_{SW}\big)u^{(k-1)} + 6h^2 f\left(u^{(k-1)}, x, y\right),$$

defines

$$\begin{aligned} u^{(k)} = {} & \big(6\boldsymbol{I} - \boldsymbol{E}_N - \boldsymbol{E}_s\big)^{-1}\big(\boldsymbol{E}_{NE} + \boldsymbol{E}_{NW} + \boldsymbol{E}_{SE} + \boldsymbol{E}_{SW}\big)u^{(k-1)} \\ & + 6h^2\big(6\boldsymbol{I} - \boldsymbol{E}_N - \boldsymbol{E}_s\big)^{-1} f(u^{(k-1)}, x, y). \end{aligned} \tag{4.2}$$

We omit further discussion about quantitative behavior of the preconditioner, but mention that a complete set of eigen basis of the preconditioner Eq. (4.1) consists of direct sums of univariate Fourier vectors, while the functional iteration operator Eq. (4.2) involves Fourier basis of mixed types of alternating sign (Appendix A.3) .

4.2. Lattice of three-color FVs

To further accelerate the convergence in an iterative procedure on configurations (as subsets) of lattices shown in Figs. 1(c) and 1(d), we propose the following.

Algorithm 4.1. *(Three-color algorithm.) With $i, j = 1, 2, \cdots$, we define color $\in \{0, 1, 2\}$ at each FV (center) of a Cartesian lattice of type I or II hexagons, respectively, by the (C-language) expressions,*

$$\big(j + 1 - 2 * (i\%2)\big)\%3 \quad \text{and} \quad \big(i + 1 - 2 * (j\%2)\big)\%3\,.$$

We assign three colors to Hex FVs, which can be used in both static and time-dependent problems. Gauss-Seidel (GS) type methods are usually applied in the natural order. However, we can rearrange the order of updates *by colors*. Variations are further investigated in §5.

https://doi.org/10.4208/nmtma.2017.m1527 Published online by Cambridge University Press

Remark 4.1.

1. In applications involving irregular regions, a net of hexagons is embedded as a subset of a (Cartesian) lattice of hexagons. The (inherited) coloring algorithm applies as well.

2. The *three-color ordering* update in a net of Hex FVs is applicable in a parallel setup. The model of parallel computation better be SPMD (*single-program-multiple-data*) with shared memory. Without giving the algorithmic details, we note that for faster convergence, part of the computation in a time march may demand for synchronous (Jac) update while the others need asynchronous (GS) update (and optionally an SOR post-processing). The multicolor update algorithm may help in this respect.

Numerical work are reported in Table 5.

5. Numerical Experiments and Discussions

Subsequent computational studies are unified in using matrix-free stencils and nonlinear Gauss-Seidel procedure (SS) in the form of Eqs. (3.33) and (3.35a). Statistics reported in tables below may include the errors (Err_M and Err_2, in discrete maximal or normalized 2-norm), the iteration counts (Iter), and the cpu-time spent (cpu-t). Both linear and semilinear anisotropic Poisson equations are investigated. All computations are enforced with $tol_x = 1.0e-15$ for Cauchy convergence, instead of residual reduction.

We describe below the test problems.

- Two anisotropic Poisson equations.

  These are modified from model problems A and G in *Ellpack* [23], on region $[0,1]^2$ and $[1,2]^2$ respectively. We adopt the analytic solutions from the source. These two equations are named as A and G in tables.

- A Helmholtz equation (marked H in tables) : $-D_1u_{xx} - D_2u_{yy} + \lambda u = f_1(x,y)$ (adapted from model problem C in *Ellpack* on $[0,1]^2$).

  With a chosen parameter $\lambda = 25$, the solution exhibits a narrow boundary layer. Similar results (not shown) were obtained with different choices of λ.

- A semilinear equation : $-D_1u_{xx} - D_2u_{yy} + u^2 = f_1(x,y)$.

  This problem is set up by using the analytic solution $u(x,y) = e^{\sin\pi x \sin\pi y}$, which helps to examine the order of approximation of discretization. It is refered to as equation Q in tables.

We explain more about the experiments and summarize our observations.

- Table 3. Approximation powers (orders) of the discrete models and accuracies in the calculated results are investigated, using SS and linear iterative method BCRs in

https://doi.org/10.4208/nmtma.2017.m1527 Published online by Cambridge University Press

Table 3: Approximations and Accuracies of seven-point methods on Hex I grids in solving anisotropic Poisson equations with $D_1 = 1.0, D_2 = 2.0$. Residuals of the discrete models are obtained using analytic solutions before the problem solving, while errors calculated after the computations, all measured in both discrete maximal and normalized 2-norm.

Eq	Sch	$n_x = n_y$	Res_M	Res_2	Res_M Ratio	Err_M	Err_2	Err_M Ratio
A	H7	20	1.84e-01	2.95e-02		8.66e-04	2.85e-04	
A	H7	40	5.06e-02	7.59e-03	3.64	2.06e-04	6.56e-05	4.20
A	H7	80	1.33e-02	1.93e-03	3.82	5.01e-05	1.57e-05	4.12
A	H7c	20	1.05e-01	2.21e-02		9.11e-04	4.39e-04	
A	H7c	40	2.80e-02	5.63e-03	3.73	2.20e-04	1.04e-04	4.13
A	H7c	80	7.27e-03	1.42e-03	3.86	5.43e-05	2.54e-05	4.06
G	H7	20	1.04e-02	7.65e-03		4.78e-04	2.79e-04	
G	H7	40	2.66e-03	1.94e-03	3.91	1.18e-04	6.75e-05	4.04
G	H7	80	6.72e-04	4.89e-04	3.95	2.94e-05	1.66e-05	4.02
G	H7c	20	6.78e-03	5.09e-03		3.15e-04	1.84e-04	
G	H7c	40	1.73e-03	1.29e-03	3.91	7.81e-05	4.46e-05	4.04
G	H7c	80	4.38e-04	3.26e-04	3.95	1.94e-05	1.10e-05	4.02
H	H7	20	9.29e+00	2.22e+00		2.70e-02	1.21e-02	
H	H7	40	2.57e+00	5.75e-01	3.61	6.28e-03	2.77e-03	4.30
H	H7	80	6.79e-01	1.46e-01	3.79	1.51e-03	6.60e-04	4.15
H	H7c	20	9.98e-02	2.40e-02		2.91e-04	1.30e-04	
H	H7c	40	7.01e-03	1.57e-03	14.24	1.71e-05	7.51e-06	17.00
H	H7c	80	4.66e-04	1.01e-04	15.04	1.04e-06	4.52e-07	16.47
Q	H7	20	9.01e-01	2.28e-01		1.03e-02	3.29e-03	
Q	H7	40	2.34e-01	5.78e-02	3.86	2.64e-03	8.28e-04	3.92
Q	H7	80	5.92e-02	1.45e-02	3.95	6.65e-04	2.08e-04	3.97
Q	H7c	20	1.09e-01	3.45e-02		1.42e-03	5.03e-04	
Q	H7c	40	3.06e-02	9.25e-03	3.56	3.75e-04	1.28e-04	3.77
Q	H7c	80	7.91e-03	2.36e-03	3.87	9.55e-05	3.23e-05	3.93

modified sparse row (MSR) format [24] as an optional double check.

Observation.

The order of discretizations by H7 and H7c schemes are illustrated in residuals (the Res_M and Res_2 columns) obtained using the analytic solutions. The residual reduction (the *Ratio* column) in maximal norm confirms our theory (the functional and the formal Taylor series approaches). The consistent error patterns shown in the

https://doi.org/10.4208/nmtma.2017.m1527 Published online by Cambridge University Press

Table 4: Hex FVs and preference in the ratio $D_2/D_1 \overset{>}{<} 1$

Eq.	Hex	Sch	D_1, D_2		$n_x = n_y$	Error_M	Error_2	Accuracy
A	I	H7	1.0	2.0	20	8.6606e-04	2.8456e-04	
A	I	H7	1.0	2.0	160	1.2340e-05	3.8516e-06	more
A	I	H7	2.0	1.0	20	2.5324e-03	1.0729e-03	
A	I	H7	2.0	1.0	160	3.7409e-05	1.5337e-05	less
A	I	H7c	1.0	2.0	20	9.1053e-04	4.3926e-04	
A	I	H7c	1.0	2.0	160	1.3453e-05	6.2691e-06	more
A	I	H7c	2.0	1.0	20	1.2204e-03	5.7477e-04	
A	I	H7c	2.0	1.0	160	1.8334e-05	8.3327e-06	less
G	I	H7	1.0	2.0	20	4.7771e-04	2.7871e-04	
G	I	H7	1.0	2.0	160	7.3388e-06	4.1166e-06	more
G	I	H7	2.0	1.0	20	9.2399e-04	5.4433e-04	
G	I	H7	2.0	1.0	160	1.4152e-05	8.0609e-06	less
G	I	H7c	1.0	2.0	20	3.1522e-04	1.8437e-04	
G	I	H7c	1.0	2.0	160	4.8410e-06	2.7226e-06	more
G	I	H7c	2.0	1.0	20	4.0616e-04	2.3932e-04	
G	I	H7c	2.0	1.0	160	6.2165e-06	3.5425e-06	less
H	I	H7c	1.0	2.0	20	2.9109e-04	1.3010e-04	
H	I	H7c	1.0	2.0	160	6.4052e-08	2.7669e-08	less
H	I	H7c	2.0	1.0	20	9.4923e-05	3.5828e-05	
H	I	H7c	2.0	1.0	160	2.1926e-08	7.9512e-09	more
Q	I	H7	1.0	2.0	20	1.0329e-02	3.2938e-03	
Q	I	H7	1.0	2.0	160	1.6693e-04	5.2031e-05	more
Q	I	H7	2.0	1.0	20	1.1310e-02	3.6766e-03	
Q	I	H7	2.0	1.0	160	1.8240e-04	5.7840e-05	less
Q	I	H7c	1.0	2.0	20	1.4151e-03	5.0287e-04	
Q	I	H7c	1.0	2.0	160	2.4020e-05	8.0867e-06	more
Q	I	H7c	2.0	1.0	20	2.1718e-03	7.2742e-04	
Q	I	H7c	2.0	1.0	160	3.3848e-05	1.1116e-05	less

right-most three columns in the table further validates our developed theory and implementation of software. We note some specific details. Compared to H7 results, the H7c scheme (i) converges as of fourth-order on the Helmholtz problem, and (ii) produces about two-thirds of the errors on problem G, and one-sixth on problem Q, but inferior on problem A. We mention on the compact scheme that, even with the *linear* (λu) term in the equation, the nontrivial choice of R_j's in Theorem 2.5 (as generalization of Theorem 2.4) must be used instead of the trivial one,

https://doi.org/10.4208/nmtma.2017.m1527 Published online by Cambridge University Press

- Table 4. Preferences for using whether Hex I or II FVs in cases of different (D_2/D_1)-ratios are studied. Due to the *irrational* relation in the coordinates, comparisons between lattices of the two types are not easy.

  Principle of symmetry.

  We handle this difficulty by reflection principle : we set the approximated squares by reflection for Hex I and II FVs, so that a discrete model on the former with $D_1/D_2 = 1/2$ shall yield *same* computation as on the latter with $D_1/D_2 = 2/1$. Still some minor differences are, (i) in the ordering by column of unstructured grid approach in the software (Figs. 1(a) vs 1(b)), which causes no significant difference in propagation errors in our tests, and (ii) the approximated domains are more like general rectangles than squares, but fair to both Hex FVs in comparisons. Indeed, the computational solutions of such dual pair are identical up to about six significant digits. Therefore, we report in the table only results with Hex I and the ratio $(D_1/D_2) = 1/2$ and 2.

  Observation.

  For standard problems (A and G), computation on Hex I with $D_2 > D_1$ are slightly more advantageous than with $D_2 < D_1$, both in the residuals (theoretic effectiveness of the discrete model, not shown) and in the errors in the calculated solutions. The preference remains with the semilinear problem (Q), but on the opposite with the Helmholtz (H).

- Table 5. Efficiencies in terms of wall-clock time are reported here. Also investigated are the accuracies in the calculated solutions using four variants of SS : GS, symmetric GS (SGS), and their three-color variants, 3cGS and 3cSGS. All are conducted on both type I and II Hex FVs.

  Observation.

  For both H7 and H7c schemes, the calculated solutions are practically the same with the four variants of SS examined here. Because of stringent stopping criteria, the GS and three-color SS (3cGS) methods yield identical solutions (up to 14 digits), and differ only in iteration counts and cpu-time spent. Details shown in the table indicates that the (simple) 3cGS is the most economic method, then 3cSGS and SGS, while GS the worst. The performance of 3cSGS is not better than 3cGS. We mention the work [13] in the context of orthogonal grid for similar unexpected results. We note the data structure (storage scheme) in our design is not particularly optimized for the three-color algorithm. This suggests the three-color algorithm is superior to (any combination of) Jac (or GS) in natural order in parallel computation, when spatial domain decomposition (DD) is applied.
  As for the cost-performance tradeoffs, the results (in coarse grid vs fine grid) favors the usage of H7c than H7 scheme, in cases of problems H and Q. The last two rows in each block of data stress again the point that the H7 scheme is much inferior to H7c scheme in accuracies.

https://doi.org/10.4208/nmtma.2017.m1527 Published online by Cambridge University Press

Table 5: Efficiencies of seven-point methods in solving anisotropic (semi)linear Poisson equations, with three-color vs regular ordering, using four variants of SS on Hex FVs. $D_1 = 1.0, D_2 = 0.5$.

Hex	Eq	Sch	$n_x = n_y$	Err_M	Err_2	Iter, GS	cpu-t GS	Iter, SGS	cpu-t SGS	Iter, 3cSGS	cpu-t 3cSGS	Iter, 3cGS	cpu-t 3cGS
II	A	H7c	100	3.46e-05	1.61e-05	25158	4.08	26554	3.79	42216	3.67	25165	3.21
II	G	H7c	100	1.24e-05	7.00e-06	28885	4.67	30182	4.31	48082	4.19	28869	3.70
II	H	H7c	100	5.39e-08	2.14e-08	8370	1.91	8820	1.75	14004	1.70	8348	1.45
II	Q	H7c	100	5.53e-05	1.82e-05	21175	5.15	22430	4.72	35522	4.66	21119	4.01
II	A	H7	100	3.18e-05	9.98e-06	25158	4.07	26558	3.80	42214	3.70	25151	3.20
II	G	H7	100	1.88e-05	1.05e-05	29167	4.72	30418	4.35	48526	4.25	29144	3.71
II	H	H7	100	1.27e-04	5.50e-05	8371	1.37	8818	1.27	14004	1.24	8349	1.09
II	Q	H7	100	3.87e-04	1.17e-04	21213	3.63	22288	3.38	35582	3.27	21194	2.81
II	H	H7	200	3.14e-05	1.35e-05	31573	20.91	33286	19.38				
II	Q	H7	200	9.71e-05	2.95e-05	80973	55.80	85504	52.14				
I	A	H7c	100	4.71e-05	2.14e-05	22994	3.81	22990	3.33	38562	3.27	22966	2.85
I	G	H7c	100	3.55e-06	2.04e-06	26218	4.34	26076	3.78	43654	3.71	26205	3.25
I	H	H7c	100	1.16e-07	4.07e-08	8118	1.87	8116	1.63	13592	1.61	8098	1.39
I	Q	H7c	100	7.86e-05	2.53e-05	19814	4.88	19836	4.21	32978	4.23	19767	3.67
I	A	H7	100	9.62e-05	3.95e-05	22989	3.81	22986	3.32	38546	3.27	22982	2.86
I	G	H7	100	8.37e-06	4.82e-06	26381	4.36	26212	3.79	43922	3.72	26369	3.27
I	H	H7	100	3.27e-04	1.16e-04	8119	1.37	8116	1.18	13596	1.18	8098	1.05
I	Q	H7	100	4.23e-04	1.31e-04	19748	3.46	19742	3.03	33112	2.96	19747	2.58
I	H	H7	200	8.12e-05	2.88e-05	30638	20.80	30614	17.99				
I	Q	H7	200	1.06e-04	3.29e-05	75589	53.45	75400	46.56				

6. Conclusions

Both a second-order ordinary and an almost fourth-order compact seven-point methods of two-dimensional anisotropic Laplacian are studied in hexagonal grid approach on two types of hexagonal grid, together with a three-color algorithm developed for use in an iterative update procedure.

In case of standard Laplacian ($D_1 = D_2$), the stencil stability condition are satisfied for all phase angles. In applications involving anisotropic Laplacian, we can safely adopt either type I or II net of hexagons provided that

$$\frac{1}{3} < \frac{D_2}{D_1} < 3.$$

Otherwise, either $\frac{D_2}{D_1} \geq 3$ or $\frac{D_2}{D_1} \leq \frac{1}{3}$, then we choose to apply type I hexagons in the former case and type II hexagons in the latter. The hexagonal grid methods never fail the stability in this sense. Analysis of these methods in solving nonlinear problems are accomplished by managing using uniform boundedness principle, with global convergence analyzed for some test problems.

These hexagonal seven-point methods, with the established theoretic stabilities and accuracies, are numerically confirmed in both linear and semilinear anisotropic Poisson problems, and can be applied also in time-dependent problems and in many applications in two-dimensional irregular domains.

https://doi.org/10.4208/nmtma.2017.m1527 Published online by Cambridge University Press

Appendix: Q_3^{Hex} and Fourier vectors of mixed types

To support Theorem 3.1, we recall for convenience the (symmetric) matrix,

$$\boldsymbol{Q}_3^{\mathrm{Hex}} := 6\boldsymbol{I} + \boldsymbol{E}_N + \boldsymbol{E}_S - 2\boldsymbol{E}_{NE}^{\mathrm{H}} - 2\boldsymbol{E}_{SW}^{\mathrm{H}} - 2\boldsymbol{E}_{NW}^{\mathrm{H}} - 2\boldsymbol{E}_{SE}^{\mathrm{H}}$$

related to an n_x-by-n_y cartesian net of a type I hexagonal grid (Figs. 1(a) and 2(a)), and consider one closely related symmetric operator, but on an orthogonal rectangular grid,

$$\boldsymbol{Q}_3^{\mathrm{Quad}} := 6\boldsymbol{I} + \boldsymbol{E}_N + \boldsymbol{E}_S - 2\boldsymbol{E}_E - 2\boldsymbol{E}_W - \boldsymbol{E}_{NE}^{\mathrm{Q}} - \boldsymbol{E}_{SW}^{\mathrm{Q}} - \boldsymbol{E}_{NW}^{\mathrm{Q}} - \boldsymbol{E}_{SE}^{\mathrm{Q}}. \tag{A.1}$$

The four diagonal incidence matrices are superscripted to make distinctions between hexagonal and quadrangular setups of nodes and the corresponding discrete neighborhood topologies, while each of the other unsuperscripted incidence matrices has unique interpretation.

We prove in the sequel that these two operators are all (symmetric and) positive definite, in subsections A.2 and A.3 (Eqs. (A.15), (A.16) and (A.18)).

A.1. Numerical Evidences

That all eigen values of the matrix $\boldsymbol{Q}_3^{\mathrm{Hex}}$ are positive is numerically checked with extremal values shown in Table 6 for some cases, together with the spectral range of discrete seven-point negative standard Laplacian ($\boldsymbol{Q}_{2s}$). The category of FV nodes in the Table indicates some modifications on the main diagonal of matrix, according to homogeneous Dirichlet boundary condition (BC). The category of FD nodes applies no such BC feedback. In cases of anisotropic Laplacian with various diffusivities ($D_1 \neq D_2$), extremal spectral values are shown in Table 7, with no BC feedback. All the matrices considered in these tables are real symmetric and the *jacobi* algorithm in [22] is used for solving the eigen systems. The resulting eigen pairs are all doubly checked by *C*-code in a straight forward manner.

Table 6: Maximal and minimal eigen values of two seven-point standard Laplacian related matrices, $\boldsymbol{Q}_3^{\mathrm{Hex}}$ and $\boldsymbol{Q}_{2s}$, the latter being the scaled discrete negative seven-point standard Laplacian defined by Eq. (3.32).

nx, ny		$\boldsymbol{Q}_3^{\mathrm{Hex}}$,	FD nodes	$\boldsymbol{Q}_{2s}$,	FD nodes	$\boldsymbol{Q}_3^{\mathrm{Hex}}$,	FV nodes	$\boldsymbol{Q}_{2s}$,	FV nodes
		max	min	max	min	max	min	max	min
4	4	13.673	1.473	8.395	1.364	15.233	1.973	10.691	2.051
6	6	14.789	0.778	8.666	0.708	15.604	0.935	10.644	0.942
8	8	15.264	0.477	8.795	0.431	15.759	0.534	10.640	0.536
10	10	15.506	0.322	8.865	0.289	15.839	0.337	10.640	0.345
4	6	14.075	1.433	8.498	1.065	15.613	2.014	10.670	1.564
6	4	14.364	0.790	8.569	1.019	15.222	0.945	10.660	1.447
8	10	15.350	0.475	8.826	0.367	15.840	0.534	10.640	0.452
10	8	15.419	0.322	8.832	0.353	15.758	0.334	10.640	0.429

https://doi.org/10.4208/nmtma.2017.m1527 Published online by Cambridge University Press

Table 7: Maximal and minimal eigen values of the discrete seven-point negative anisotropic Laplacian ($\mathbf{Q}_{2a}$) as defined by Eq. (3.20).

nx, ny		D1=1.0 , D2=2.0		D1=1.0 , D2=3.0		D1=2.0 , D2=1.0		D1=3.0 , D2=1.0	
		max	min	max	min	max	min	max	min
4	4	13.492	1.957	18.879	2.542	14.293	2.124	21.123	2.877
6	6	13.880	1.014	19.521	1.317	15.105	1.107	22.498	1.503
8	8	14.072	0.616	19.786	0.800	15.454	0.674	23.084	0.916
10	10	14.189	0.413	19.924	0.536	15.633	0.452	23.385	0.615
4	6	13.826	1.371	19.479	1.674	14.391	1.821	21.426	2.574
6	4	13.554	1.613	18.934	2.199	14.984	1.433	22.160	1.840
8	10	14.173	0.491	19.915	0.614	15.476	0.609	23.150	0.850
10	8	14.090	0.538	19.795	0.722	15.609	0.518	23.318	0.682

A.2. Q_3^{Quad} is S.P.D.

For our purpose, we assume n_x and n_y are even, and consider in current subsection an n_x-by-n_y two-dimensional (2D) orthogonal cartesian grid consisting of cell-center nodes

$$\left\{ (x_i, y_j) \,\middle|\, x_i = \frac{i-0.5}{n_x},\ y_j = \frac{j-0.5}{n_y},\ 1 \le i \le n_x,\ 1 \le j \le n_y \right\}.$$

Note firstly the one-dimensional (1D) Fourier vectors, with $n = n_x$ or $n = n_y$,

$$\begin{aligned} v^l &:= \left(v_i^l\right)_{i=1}^n \equiv \left(\sin l(i-0.5)\pi/n\right)_{i=1}^n, && 1 \le l \le n, \\ u^l &:= \left(u_i^l\right)_{i=1}^n \equiv \left(\cos(l-1)(i-0.5)\pi/n\right)_{i=1}^n, && 1 \le l \le n, \end{aligned}$$

together with the 1D orthogonality relations

$$\langle v^l, v^p \rangle = \begin{cases} n, & l = p = n, \\ \frac{n}{2}, & 1 \le l = p < n, \\ 0, & \text{otherwise}, \end{cases} \qquad \langle u^l, u^p \rangle = \begin{cases} n, & 1 = l = p, \\ \frac{n}{2}, & 1 < l = p \le n, \\ 0, & \text{otherwise}, \end{cases} \tag{A.2}$$

and the 1D cross-orthogonality

$$\langle v^l, u^p \rangle = \begin{cases} 0, & \text{if } l-p \text{ is odd}, \\ \frac{1}{2}\left(\csc \frac{(l+p-1)\pi}{2n} + \csc \frac{(l-p+1)\pi}{2n} \right), & \text{otherwise}. \end{cases} \tag{A.3}$$

Basis sets exist in various forms, we state only those actually used in subsequent applications.

Lemma A.1. *Any one of the following sets forms a (complete) basis of* $\mathbb{R}^n$.

$$\begin{aligned} &(1)\ \{ v^l \mid 1 \le l \le n \}, && (3)\ \{ v^{2l-1},\ u^{2l} \mid 1 \le l \le \tfrac{n}{2} \}, \\ &(2)\ \{ u^l \mid 1 \le l \le n \}, && (4)\ \{ \left((-1)^i v_i^l\right)_{i=1}^n \mid 1 \le l \le n \}. \end{aligned}$$

https://doi.org/10.4208/nmtma.2017.m1527 Published online by Cambridge University Press

The extension that $v^0 = u^{n+1} = 0$ is noted. Let

$$1 \le l,\ \ i \le n_x,\ \ 1 \le m,\ \ j \le n_y,$$

the 2D Fourier Sine and Cosine vectors are

$$v^{l,m} := \{v_{i,j}^{l,m}\}_{i,j}, \qquad v_{i,j}^{l,m} \equiv v_i^l \cdot v_j^m \equiv \sin(l\pi x_i) \cdot \sin(m\pi y_j), \tag{A.4a}$$

$$u^{l,m} := \{u_{i,j}^{l,m}\}_{i,j}, \qquad u_{i,j}^{l,m} \equiv u_i^l \cdot u_j^m \equiv \cos((l-1)\pi x_i) \cdot \cos((m-1)\pi y_j) \tag{A.4b}$$

with the convenience that

$$v^{l,m} \equiv 0, \ \text{ if } \ lm = 0, \quad \text{and} \quad u^{l,m} \equiv 0, \ \text{ if } \ l = n_x + 1, \ \text{ or } \ m = n_y + 1. \tag{A.5}$$

Note the 2D orthogonality relations

$$\langle v^{l,m}, v^{p,q} \rangle = \langle v^l, v^p \rangle \ \langle v^m, v^q \rangle = \begin{cases} n_x n_y, & l = p = n_x, \quad m = q = n_y, \\ \frac{n_x n_y}{2}, & l = p = n_x, \quad m = q < n_y, \\ \frac{n_x n_y}{2}, & l = p < n_x, \quad m = q = n_y, \\ \frac{n_x n_y}{4}, & l = p < n_x, \quad m = q < n_y, \\ 0, & \text{otherwise}, \end{cases}$$

$$\langle u^{l,m}, u^{p,q} \rangle = \langle u^l, u^p \rangle \ \langle u^m, u^q \rangle = \begin{cases} n_x n_y, & 1 = l = p, \quad 1 = m = q, \\ \frac{n_x n_y}{2}, & 1 = l = p, \quad 1 < m = q, \\ \frac{n_x n_y}{2}, & 1 < l = p, \quad 1 = m = q, \\ \frac{n_x n_y}{4}, & 1 < l = p, \quad 1 < m = q, \\ 0, & \text{otherwise}, \end{cases}$$

and the 2D cross-orthogonality

$$\langle v^{l,m}, u^{p,q} \rangle = \langle v^l, u^p \rangle \ \langle v^m, u^q \rangle = \begin{cases} 0, & \text{if either (l-p) or (m-q) is odd ,} \\ \alpha, & \text{if both (l-p) and (m-q) are even.} \end{cases}$$

Here

$$\alpha = \frac{1}{4} \left(\csc \frac{(l+p-1)\pi}{2n_x} + \csc \frac{(l-p+1)\pi}{2n_x} \right) \left(\csc \frac{(m+q-1)\pi}{2n_y} + \csc \frac{(m-q+1)\pi}{2n_y} \right).$$

We need the following options of choosing a basis.

https://doi.org/10.4208/nmtma.2017.m1527 Published online by Cambridge University Press

Lemma A.2. *With $1 \le i \le n_x$, $1 \le j \le n_y$, any one of the following sets generates a basis of $\mathbb{R}^{n_x n_y}$:*

$$
\begin{aligned}
&(1a)\quad \left\{ \left(v_i^l v_j^m\right)_{i,j} \;\middle|\; 1 \le l \le n_x,\quad 1 \le m \le n_y \right\},\\
&(1b)\quad \left\{ \left(u_i^l u_j^m\right)_{i,j} \;\middle|\; 1 \le l \le n_x,\quad 1 \le m \le n_y \right\},\\
&(2a)\quad \left\{ \left(v_i^l v_j^{2m-1}\right)_{i,j}, \left(v_i^l u_j^{2m}\right)_{i,j} \;\middle|\; 1 \le l \le n_x,\quad 1 \le m \le \tfrac{n_y}{2} \right\},\\
&(2b)\quad \left\{ \left(u_i^l v_j^{2m-1}\right)_{i,j}, \left(u_i^l u_j^{2m}\right)_{i,j} \;\middle|\; 1 \le l \le n_x,\quad 1 \le m \le \tfrac{n_y}{2} \right\},\\
&(3a)\quad \left\{ \left(v_i^l v_j^{2m-1}\right)_{i,j}, \left(u_i^l u_j^{2m}\right)_{i,j} \;\middle|\; 1 \le l \le n_x,\quad 1 \le m \le \tfrac{n_y}{2} \right\},\\
&(3b)\quad \left\{ \left(v_i^{2l-1} v_j^m\right)_{i,j}, \left(u_i^{2l} u_j^m\right)_{i,j} \;\middle|\; 1 \le l \le \tfrac{n_x}{2},\quad 1 \le m \le n_y \right\},\\
&(4a)\quad \left\{ \left((-1)^i v_i^l v_j^{2m-1}\right)_{i,j}, \left(v_i^l u_j^{2m}\right)_{i,j} \;\middle|\; 1 \le l \le n_x,\quad 1 \le m \le \tfrac{n_y}{2} \right\},\\
&(4b)\quad \left\{ \left((-1)^i v_i^l u_j^{2m}\right)_{i,j}, \left(v_i^l v_j^{2m-1}\right)_{i,j} \;\middle|\; 1 \le l \le n_x,\quad 1 \le m \le \tfrac{n_y}{2} \right\}.
\end{aligned}
$$

One of these basis set is specified in each of subsequent applications, guided partially by *even-odd parities* of the 2D Fourier vectors. As an illustration of the pattern in option (3a),

$$
\begin{aligned}
\mathbb{R}^{n_x n_y} =& \operatorname{span}\left\{ v_i^l v_j^{2m-1},\ u_i^l u_j^{2m} \;\middle|\; 1 \le l \le n_x,\ 1 \le m \le n_y/2 \right\}\\
\equiv& \left\{ u_i^1 u_j^{2m} \;\middle|\; 1 \le m \le n_y/2 \right\}\\
&\bigoplus \left\{ v_i^{n_x} v_j^{2m-1} \;\middle|\; 1 \le m \le n_y/2 \right\}\\
&\bigoplus \left\{ v_i^l v_j^{2m-1},\ u_i^{l+1} u_j^{2m} \;\middle|\; 1 \le l \le n_x - 1,\ 1 \le m \le n_y/2 \right\}. \qquad \text{(A.7)}
\end{aligned}
$$

We mention several operators not superscripted for ease of reading in this subsection.

Vertical symmetric shift.

$$
\left(\boldsymbol{E}_N + \boldsymbol{E}_s\right) v^{l,m} = 2\cos\frac{m\pi}{n_y} v^{l,m}, \qquad \text{(A.8a)}
$$

$$
\left(\boldsymbol{E}_N + \boldsymbol{E}_s\right) u^{l,m} = 2\cos\frac{(m-1)\pi}{n_y} u^{l,m}. \qquad \text{(A.8b)}
$$

Horizontal symmetric shift.

$$
\left(\boldsymbol{E}_E + \boldsymbol{E}_w\right) v^{l,m} = 2\cos\frac{l\pi}{n_x} v^{l,m}, \qquad \text{(A.9a)}
$$

$$
\left(\boldsymbol{E}_E + \boldsymbol{E}_w\right) u^{l,m} = 2\cos\frac{(l-1)\pi}{n_x} u^{l,m}. \qquad \text{(A.9b)}
$$

Four-way diagonal symmetric shift.

$$
\left(\boldsymbol{E}_{NE} + \boldsymbol{E}_{NW} + \boldsymbol{E}_{sE} + \boldsymbol{E}_{sW}\right) v^{l,m} = 2\alpha_{l,m} v^{l,m}, \qquad \text{(A.10a)}
$$

$$
\left(\boldsymbol{E}_{NE} + \boldsymbol{E}_{NW} + \boldsymbol{E}_{sE} + \boldsymbol{E}_{sW}\right) u^{l,m} = 2\alpha_{l-1,m-1} u^{l,m}, \qquad \text{(A.10b)}
$$

https://doi.org/10.4208/nmtma.2017.m1527 Published online by Cambridge University Press

in which $\alpha_{l,m} := 2\cos\frac{l\pi}{n_x}\cos\frac{m\pi}{n_y}$.

We need also the next two non-symmetric operators. Both are actually direct sums of (scaled) rotations.

Vertical forward average.

$$(\boldsymbol{E}_{NE}+\boldsymbol{E}_{NW})\ v_{i,j}^{l,m} = 2\cos\frac{l\pi}{n_x}v_{i,j+1}^{l,m}, \tag{A.11a}$$

$$(\boldsymbol{E}_{NE}+\boldsymbol{E}_{NW})\ u_{i,j}^{l,m} = 2\cos\frac{(l-1)\pi}{n_x}u_{i,j+1}^{l,m}, \tag{A.11b}$$

$$(\boldsymbol{E}_{NE}+\boldsymbol{E}_{NW})\ v_i^l u_j^m = 2\cos\frac{l\pi}{n_x}v_i^l u_{j+1}^m, \tag{A.11c}$$

$$(\boldsymbol{E}_{NE}+\boldsymbol{E}_{NW})\ u_i^l v_j^m = 2\cos\frac{(l-1)\pi}{n_x}u_i^l v_{j+1}^m. \tag{A.11d}$$

Vertical backward average.

$$(\boldsymbol{E}_{SE}+\boldsymbol{E}_{SW})\ v_{i,j}^{l,m} = 2\cos\frac{l\pi}{n_x}v_{i,j-1}^{l,m}, \tag{A.12a}$$

$$(\boldsymbol{E}_{SE}+\boldsymbol{E}_{SW})\ u_{i,j}^{l,m} = 2\cos\frac{(l-1)\pi}{n_x}u_{i,j-1}^{l,m}, \tag{A.12b}$$

$$(\boldsymbol{E}_{SE}+\boldsymbol{E}_{SW})\ v_i^l u_j^m = 2\cos\frac{l\pi}{n_x}v_i^l u_{j-1}^m, \tag{A.12c}$$

$$(\boldsymbol{E}_{SE}+\boldsymbol{E}_{SW})\ u_i^l v_j^m = 2\cos\frac{(l-1)\pi}{n_x}u_i^l v_{j-1}^m. \tag{A.12d}$$

These are actually direct sums of (scaled) rotations. That is, by further expansion with $\gamma_{l,m} := 2\cos\frac{l\pi}{n_x}\sin\frac{m\pi}{n_y}$,

$$(\boldsymbol{E}_{NE}+\boldsymbol{E}_{NW})\ v_i^l v_j^m = \alpha_{l,m}\, v_i^l v_j^m + \gamma_{l,m}\, v_i^l u_j^{m+1}, \tag{A.13a}$$

$$(\boldsymbol{E}_{NE}+\boldsymbol{E}_{NW})\ v_i^l u_j^{m+1} = -\gamma_{l,m}\, v_i^l v_j^m + \alpha_{l,m}\, v_i^l u_j^{m+1}, \tag{A.13b}$$

$$(\boldsymbol{E}_{SE}+\boldsymbol{E}_{SW})\ v_i^l v_j^m = \alpha_{l,m}\, v_i^l v_j^m - \gamma_{l,m}\, v_i^l u_j^{m+1}, \tag{A.13c}$$

$$(\boldsymbol{E}_{SE}+\boldsymbol{E}_{SW})\ v_i^l u_j^{m+1} = \gamma_{l,m}\, v_i^l v_j^m + \alpha_{l,m}\, v_i^l u_j^{m+1}, \tag{A.13d}$$

and

$$(\boldsymbol{E}_{NE}+\boldsymbol{E}_{NW})\ u_i^l u_j^m = \alpha_{l-1,m-1}\, u_i^l u_j^m - \gamma_{l-1,m-1}\, u_i^l v_j^{m-1}, \tag{A.14a}$$

$$(\boldsymbol{E}_{NE}+\boldsymbol{E}_{NW})\ u_i^l v_j^{m-1} = \gamma_{l-1,m-1}\, u_i^l u_j^m + \alpha_{l-1,m-1}\, u_i^l v_j^{m-1}, \tag{A.14b}$$

$$(\boldsymbol{E}_{SE}+\boldsymbol{E}_{SW})\ u_i^l u_j^m = \alpha_{l-1,m-1}\, u_i^l u_j^m + \gamma_{l-1,m-1}\, u_i^l v_j^{m-1}, \tag{A.14c}$$

$$(\boldsymbol{E}_{SE}+\boldsymbol{E}_{SW})\ u_i^l v_j^{m-1} = -\gamma_{l-1,m-1}\, u_i^l u_j^m + \alpha_{l-1,m-1}\, u_i^l v_j^{m-1}. \tag{A.14d}$$

https://doi.org/10.4208/nmtma.2017.m1527 Published online by Cambridge University Press

The fact that $\boldsymbol{Q}_3^{\text{Quad}}$ (Eq. (A.1)) is a diagonal operator with positive eigen values is justified in a straight forward manner, as follows.

Theorem A.1. *$\boldsymbol{Q}_3^{\text{Quad}}$ is (symmetric and) positive definite.*

Proof. By Eqs. (A.8)– (A.10), we have

$$\boldsymbol{Q}_3^{\text{Quad}} \cdot v^{l,m} = \lambda_{l,m} \cdot v^{l,m}, \qquad 1 \le l \le n_x, \qquad 1 \le m \le n_y, \tag{A.15a}$$

$$\boldsymbol{Q}_3^{\text{Quad}} \cdot u^{l+1,m+1} = \lambda_{l,m} \cdot u^{l+1,m+1}, \qquad 1 \le l+1 \le n_x, \qquad 1 \le m+1 \le n_y; \tag{A.15b}$$

with

$$\begin{aligned}\lambda_{l,m} &= 6 + 2\cos\frac{m\pi}{n_y} - 4\cos\frac{l\pi}{n_x} - 4\cos\frac{l\pi}{n_x}\cos\frac{m\pi}{n_y} \\ &= 4 + \left(2 + 2\cos\frac{m\pi}{n_y}\right)\left(1 - 2\cos\frac{l\pi}{n_x}\right).\end{aligned}$$

Notice that, with $n_x, n_y \ge 4$,

$$\max \lambda_{l,m} = \lambda_{n_x,1} = 10 + 6\cos\frac{\pi}{n_y} \lesssim 16,$$

$$\min \lambda_{l,m} = \lambda_{1,1} = 4 + \left(2 + 2\cos\frac{\pi}{n_y}\right)\left(1 - 2\cos\frac{\pi}{n_x}\right) > \frac{4\pi^2}{n_x^2} + \frac{\pi^2}{n_y^2} - \frac{\pi^4}{n_x^2 n_y^2} > \frac{4\pi^2}{n_x^2}.$$

This ends the proof, up to choosing the basis option (1) in Lemma A.2 or option (3) as detailed in Eq. (A.7). □

Some projection coeffcients in this and later subsections are collected in Table 8.

Table 8: Coeffcients of projections in various basis vectors. Ranges of indices are $1 \le l \le n_x$, $1 \le m \le n_y$, with $l = 0, m = 0$ allowed for convenience.

Coefficients	Values	Properties	Eqs.
$\alpha_{l,m}$	$2\cos\frac{l\pi}{n_x}\cos\frac{m\pi}{n_y}$		A.10, A.13,
$\gamma_{l,m}$	$2\cos\frac{l\pi}{n_x}\sin\frac{m\pi}{n_y}$		A.13, A.14
$\xi_{l,m}$	$4\cos\frac{l\pi}{n_x}\sin\frac{m\pi}{n_y}$	$= 2\gamma_{l,m}$	A.16, A.18
$\lambda_{l,m}$	$6 + 2\cos\frac{m\pi}{n_y} - 4\cos\frac{l\pi}{n_x}$		
	$-4\cos\frac{l\pi}{n_x}\cos\frac{m\pi}{n_y}$	> 0	A.15, A.16, A.18
$\eta_{l,m}$	$6 + 2\cos\frac{m\pi}{n_y} + 4\cos\frac{l\pi}{n_x}$		
	$+4\cos\frac{l\pi}{n_x}\cos\frac{m\pi}{n_y}$	$= \lambda_{n_x-l,m}$	A.18

https://doi.org/10.4208/nmtma.2017.m1527 Published online by Cambridge University Press

A.3. Q_3^{Hex} is S.P.D.

We consider the setup of Hex I grid and note a useful reduction.

Lemma A.3. *Concerning the four diagonal primitive incidence operators' actions in Hex I setup, the following equivalence at matrices level is valid (Fig. 1(a)).*

$$\begin{aligned} &\boldsymbol{E}_{NW}^{\mathrm{H}}, \boldsymbol{E}_{NE}^{\mathrm{H}}, \boldsymbol{E}_{SW}^{\mathrm{H}}, \boldsymbol{E}_{SE}^{\mathrm{H}} = \boldsymbol{E}_{W}^{\mathrm{Q}}, \boldsymbol{E}_{E}^{\mathrm{Q}}, \boldsymbol{E}_{SW}^{\mathrm{Q}}, \boldsymbol{E}_{SE}^{\mathrm{Q}}, && \text{resp. for grid columns } 1,3,5,\cdots \\ &\boldsymbol{E}_{SW}^{\mathrm{H}}, \boldsymbol{E}_{SE}^{\mathrm{H}}, \boldsymbol{E}_{NW}^{\mathrm{H}}, \boldsymbol{E}_{NE}^{\mathrm{H}} = \boldsymbol{E}_{W}^{\mathrm{Q}}, \boldsymbol{E}_{E}^{\mathrm{Q}}, \boldsymbol{E}_{NW}^{\mathrm{Q}}, \boldsymbol{E}_{NE}^{\mathrm{Q}}, && \text{resp. for grid columns } 2,4,6,\cdots . \end{aligned}$$

The above reduction and Eqs. (A.11)–(A.13) and (A.15) imply the following, with ξ defined in Table 8.

At odd column nodes (with odd i),

$$\begin{aligned} \boldsymbol{Q}_3^{\mathrm{Hex}}\, v_{i,j}^{l,m} &= \Big(6\boldsymbol{I} + \boldsymbol{E}_N + \boldsymbol{E}_s - 2\boldsymbol{E}_E^{\mathrm{Q}} - 2\boldsymbol{E}_W^{\mathrm{Q}}\Big)\, v_{i,j}^{l,m} - 2\Big(\boldsymbol{E}_{SW}^{\mathrm{Q}} + \boldsymbol{E}_{SE}^{\mathrm{Q}}\Big)\, v_{i,j}^{l,m} \\ &= \Big(6 + 2\cos\frac{m\pi}{n_y} - 4\cos\frac{l\pi}{n_x}\Big)\, v_{i,j}^{l,m} - 4\cos\frac{l\pi}{n_x}\, v_{i,j-1}^{l,m} \\ &= \lambda_{l,m} v_{i,j}^{l,m} + \xi_{l,m} v_i^l\, u_j^{m+1} = \boldsymbol{Q}_3^{\mathrm{Quad}}\, v_{i,j}^{l,m} + \xi_{l,m} v_i^l\, u_j^{m+1}. \end{aligned}$$

At even column nodes (with even i),

$$\begin{aligned} \boldsymbol{Q}_3^{\mathrm{Hex}}\, v_{i,j}^{l,m} &= \Big(6\boldsymbol{I} + \boldsymbol{E}_N + \boldsymbol{E}_s - 2\boldsymbol{E}_E^{\mathrm{Q}} - 2\boldsymbol{E}_W^{\mathrm{Q}}\Big)\, v_{i,j}^{l,m} - 2\Big(\boldsymbol{E}_{NW}^{\mathrm{Q}} + \boldsymbol{E}_{NE}^{\mathrm{Q}}\Big)\, v_{i,j}^{l,m} \\ &= \Big(6 + 2\cos\frac{m\pi}{n_y} - 4\cos\frac{l\pi}{n_x}\Big)\, v_{i,j}^{l,m} - 4\cos\frac{l\pi}{n_x}\, v_{i,j+1}^{l,m} \\ &= \lambda_{l,m} v_{i,j}^{l,m} - \xi_{l,m} v_i^l\, u_j^{m+1} = \boldsymbol{Q}_3^{\mathrm{Quad}}\, v_{i,j}^{l,m} - \xi_{l,m} v_i^l\, u_j^{m+1}. \end{aligned}$$

These are ortho-sums, since $(v_j^m)_{j=1:n_y} \perp (u_j^{m+1})_{j=1:n_y}$ independent of the discrete *i-space* by 1D cross-orthogonality (Eq. (A.3)). In summary,

$$\boldsymbol{Q}_3^{\mathrm{Hex}} v_i^l\, v_j^m = \lambda_{l,m}\, v_i^l\, v_j^m - \xi_{l,m}\big((-1)^i v_i^l\big)\, u_j^{m+1}, \tag{A.16a}$$

$$\boldsymbol{Q}_3^{\mathrm{Hex}} v_i^l\, u_j^{m+1} = \lambda_{l,m}\, v_i^l\, u_j^{m+1} + \xi_{l,m}\big((-1)^i v_i^l\big)\, v_j^m. \tag{A.16b}$$

The second expression above is derived by an effort parallel to that in deriving the first expression. We notice that

$$\|\boldsymbol{Q}_3^{\mathrm{Hex}}\, v_i^l v_j^m\|^2 = (\lambda_{l,m}^2 + \xi_{l,m}^2)\, \|v_i^l v_j^m\|^2, \tag{A.17a}$$

$$\|\boldsymbol{Q}_3^{\mathrm{Hex}}\, v_i^l u_j^{m+1}\|^2 = (\lambda_{l,m}^2 + \xi_{l,m}^2)\, \|v_i^l u_j^{m+1}\|^2, \tag{A.17b}$$

because

$$\|v^{l,m}\| = \|v_i^l\|\, \|v_j^m\| = \|v_i^l\|\, \|u_j^{m+1}\| = \|\big((-1)^i v_i^l\big) u_j^{m+1}\|$$

by Eq. (A.2) with $1 \le l \le n_x$ and $1 \le m, m+1 \le n_y$.

The proof below makes use of the associated bilinear form.

https://doi.org/10.4208/nmtma.2017.m1527 Published online by Cambridge University Press

Theorem A.2. $\boldsymbol{Q}_{\mathbf{3}}^{\mathrm{Hex}}$ *is (symmetric and) positive definite.*

Proof. For a basis, we choose (option (2a) in Lemma A.2)

$$\left\{ \left(v_i^l v_j^m\right)_{i,j},\ \left(v_i^l u_j^{m+1}\right)_{i,j} \ \middle|\ l=1,2,3,\cdots,n_x,\quad m=1,3,5,\cdots,n_y-1 \right\}.$$

We note choosing basis option (2b) in Lemma A.2 with ths usage of Eq. (A.14) can do as well. Owing to the 1D (cross-)orthogonalities (Eqs. (A.2,A.3)) that

$$(u_j^m)_{j=1}^{n_y} \perp (u_j^{m+1})_{j=1}^{n_y} \qquad \text{and} \qquad (v_j^m)_{j=1}^{n_y} \perp (u_j^{m+1})_{j=1}^{n_y},$$

we obtain

$$\left\langle \boldsymbol{Q}_{\mathbf{3}}^{\mathrm{Hex}} v_{i,j}^{l,m},\ v_{i,j}^{l,m} \right\rangle = \left\langle \lambda_{l,m} v_{i,j}^{l,m} - \xi_{l,m}\left((-1)^i v_i^l\right) u_j^{m+1},\ v_i^l v_j^m \right\rangle = \lambda_{l,m} \|v^{l,m}\|^2,$$
$$\left\langle \boldsymbol{Q}_{\mathbf{3}}^{\mathrm{Hex}} v_i^l u_j^{m+1},\ v_i^l u_j^{m+1} \right\rangle = \left\langle \lambda_{l,m} v_i^l u_j^{m+1} + \xi_{l,m}\left((-1)^i v_i^l\right) u_j^m,\ v_i^l u_j^{m+1} \right\rangle = \lambda_{l,m} \|v_i^l u_j^{m+1}\|^2.$$

Next, for a *simple* linear combination (with real coefficients c and d), we can derive by using Eqs. (A.16) and (A.17) that

$$\left\langle\ \boldsymbol{Q}_{\mathbf{3}}^{\mathrm{Hex}}\left(c v_{i,j}^{l,m} + d v_i^l u_j^{m+1}\right),\ \left(c v_{i,j}^{l,m} + d v_i^l u_j^{m+1}\right)\ \right\rangle\ =\ \lambda_{l,m} c^2 \|v^{l,m}\|^2 + \lambda_{l,m} d^2 \|v_i^l u_j^{m+1}\|^2.$$

Finally, $\boldsymbol{Q}_{\mathbf{3}}^{\mathrm{Hex}}$ is invariant in each of the two-dimensional j-space spanned by $\{\, v_j^m,\ u_j^{m+1} \,\}$, acting as orthogonal scaled rotations. The j-components in all $v_i^l v_j^m$ terms have odd values of m, while that in all $v_i^l u_j^{m+1}$ terms have even values of $(m+1)$. Therefore,

$$\begin{aligned}
&\left\langle\ \boldsymbol{Q}_{\mathbf{3}}^{\mathrm{Hex}} \sum_{l,m}\left(c_{l,m} v_{i,j}^{l,m} + d_{l,m} v_i^l u_j^{m+1}\right),\ \sum_{l,m}\left(c_{l,m} v_{i,j}^{l,m} + d_{l,m} v_i^l u_j^{m+1}\right)\ \right\rangle \\
=&\left\langle\ \sum_{l,m} c_{l,m}\lambda_{l,m} v_i^l v_j^m - \sum_{l,m} c_{l,m}\xi_{l,m}(-1)^i v_i^l u_j^{m+1},\ \sum_{l,m}\left(c_{l,m} v_{i,j}^{l,m} + d_{l,m} v_i^l u_j^{m+1}\right)\ \right\rangle \\
&+\left\langle\ \sum_{l,m} d_{l,m}\lambda_{l,m} v_i^l u_j^{m+1} + \sum_{l,m} d_{l,m}\xi_{l,m}(-1)^i v_i^l v_j^m,\ \sum_{l,m}\left(c_{l,m} v_{i,j}^{l,m} + d_{l,m} v_i^l u_j^{m+1}\right)\ \right\rangle \\
=&\sum_{l,m}\lambda_{l,m} c_{l,m}^2 \|v_i^l v_j^m\|^2 + \sum_{l,m}\lambda_{l,m} d_{l,m}^2 \|v_i^l u_j^{m+1}\|^2\ >\ 0.
\end{aligned}$$

The cancellations in the expansion of the bilinear form are clean because $\|u_j^{m+1}\|^2 = \|v_j^m\|^2 = \frac{n_y}{2}$ by Eq. (A.2) and $1 \le m < m+1 \le n_y$. The final positivity follows from Theorem A.1 that all $\lambda_{l,m} > 0$. This ends the proof. □

Remark A.1. Different representation of $\boldsymbol{Q}_{\mathbf{3}}^{\mathrm{Hex}}$ other than Eq. (A.16) can be derived by using basis option (4a) (or (4b)) in Lemma A.2, and then prove the above theorem accordingly. Indeed, further investigation yields

$$\boldsymbol{Q}_{\mathbf{3}}^{\mathrm{Hex}} \begin{pmatrix} v_i^l v_j^m \\ (-1)^i v_i^l u_j^{m+1} \\ (-1)^i v_i^l v_j^m \\ v_i^l u_j^{m+1} \end{pmatrix} = \begin{bmatrix} \lambda_{l,m} & -\xi_{l,m} & 0 & 0 \\ -\xi_{l,m} & \eta_{l,m} & 0 & 0 \\ 0 & 0 & \eta_{l,m} & \xi_{l,m} \\ 0 & 0 & \xi_{l,m} & \lambda_{l,m} \end{bmatrix} \begin{pmatrix} v_i^l v_j^m \\ (-1)^i v_i^l u_j^{m+1} \\ (-1)^i v_i^l v_j^m \\ v_i^l u_j^{m+1} \end{pmatrix} \tag{A.18}$$

https://doi.org/10.4208/nmtma.2017.m1527 Published online by Cambridge University Press

with

$$\eta_{l,m} = 6 + 2\cos\frac{m\pi}{n_y} + 4\cos\frac{l\pi}{n_x} + 4\cos\frac{l\pi}{n_x}\cos\frac{m\pi}{n_y} = \lambda_{n_x-l,m} > 0.$$

However, the complexity of the argument in providing an alternative proof to the theorem seemed retaining at the same level. We mention only that, using the relation

$$(-1)^{i+1}v_i^l = (-1)^{i+1}\sin\frac{l(i-0.5)\pi}{n_x} = \cos\frac{(n_x-l)(i-0.5)\pi}{n_x} = u_i^{n_x+1-l}.$$

we can establish the representation

$$\begin{aligned}
\boldsymbol{Q}_3^{\mathrm{Hex}}\ \big((-1)^i v_i^l v_j^m\big) &= \eta_{l,m}\big((-1)^i v_i^l v_j^m\big) + \xi_{l,m}\big(v_i^l u_j^{m+1}\big),\\
\boldsymbol{Q}_3^{\mathrm{Hex}}\ \big((-1)^i v_i^l u_j^{m+1}\big) &= \eta_{l,m}\big((-1)^i v_i^l u_j^{m+1}\big) - \xi_{l,m}\big(v_i^l v_j^m\big),
\end{aligned}$$

which, together with Eq. (A.16), yields Eq. (A.18).

Acknowledgements The author would like to thank the referees for the helpful suggestions, and is grateful to Tunghai university for continued laboratory support for a long period of time.

References

[1] K. Atkinson and W. Han, Theoretical Numerical Analysis : A Functional Analysis Framework, Springer-Verlag, New York, 2001.
[2] O. xelsson, Iterative Solution Methods, Cambridge University Press, 1994.
[3] F. L. Bauer and C. T. Fike, *Norms and exclusion theorems*, Numer. Math., 2 (1960), pp. 137–141.
[4] A. Berman and R. J. Plemmons, Nonnegative Matrices in the Mathematical Sciences, SIAM, Philadelphia, 1994.
[5] M. E. Bystrytskyi and M. M. Moskl'kov, *The difference Laplace operator on a seven-point nonorthogonal pattern of a rectangular grid and its spectral preperties*, J. Math. Sci., 104(6) (2001), pp. 1593–1598.
[6] R. H. F. Chan and X. Q. Jin, An Introduction to Iterative Toeplitz Solvers, SIAM, 2007.
[7] R. van Eck HJ, J. A. Kors and G. van Herpen, *The U wave in the electrocardiogram: a solution for a 100-year-old riddle*, Cardiovasc Res., 67(2) (2005), pp. 256–262.
[8] R. P. Heikes and D. A. Randall, *Numerical integration of the shallow-water equations on a twisted icosahedral grid. part I: Basic design and results of tests*, Mon. Wea. Rev., 123 (1995), pp. 1862–1880.
[9] R. P. Heikes and D. A. Randall, *Numerical integration of the shallow-water equations on a twisted icosahedral grid. part II: A detailed description of the grid and an analysis of numerical accuracy*, Mon. Wea. Rev., 123 (1995), pp. 1881–1887.
[10] R. P. Heikes, D. A. Randall, and C. S. Konor, *Optimized icosahedral grids: performance of finite-Difference operators and multigrid solver*, Mon. Wea. Rev., 141 (2013), pp. 4450–4469.
[11] R. A. Horn and C. R. Johnson, Matrix Analysis, 2nd ed., Cambridge University Press, 2013.
[12] S. Karaa and J. Zhang, *Analysis of stationary iterative methods for the discrete convection-diffusion equation with a 9-point compact scheme*, J. Comput. Appl. Math., 154 (2003), pp. 447–476.

https://doi.org/10.4208/nmtma.2017.m1527 Published online by Cambridge University Press

[13] C. C. Jay Kuo and T. F. Chan, *Two-color dourier analysis of iterative algorithms for elliptic problems with red-black ordering*, SIAM J. Sci. Stat. Comput., 11(4) (1990), pp. 767–793.
[14] D. Lee, *Complete solution to seven-point schemes of discrete anisotropic Laplacian on regular hexagons*, AADM., 9 (2015), pp. 180–197.
[15] D. Lee, H. C. Tien, C. P. Luo and H. N. Luk, *Hexagonal grid methods with applications to partial differential equations*, Int. J. of Comput. Math., 91(9) (2014), pp. 1986–2009.
[16] W. M. Pickering, *On the solution of Poisson's equation in a regular hexagonal grid using FFT methods*, J. Comput. Phys., 64 (1986), pp. 320–333.
[17] V. L. Makarov, S. V. Mararov and M. N. Moskal'kov, *Spectral properties of the difference Laplacian on a hexagonal mesh and their application*, Differ. Equ., 29(7) (1993), pp. 959–1118.
[18] B. J. McCartin, *Eigenstructure of the equilateral triangle, part I: the Dirichlet problem*, SIAM Review, 45(2) (2003), pp. 267–287.
[19] B. J. McCartin, *Eigenstructure of the equilateral triangle, part II: the Neumann problem*, Math. Probl. Eng., 8(5) (2002), pp. 517–539.
[20] S. Nickovic, M. B. Gavrilov and I. A. Tosic, *Geostrophic adjustment on hexagonal grids*, Mon. Wea. Rev., 130 (2002), pp. 668–683.
[21] P. Perona and J. Malik, *Scale-space and edge detection using anisotropic diffusion*, IEEE T. Pattern Anal., 12(2) (1990), pp. 161–192.
[22] W. H. Press, S. A. Teukolsky, W. T. Vetterling, B. P. Flannery, Numerical Recipes in C, Cambridge University Press (1992).
[23] J. R. Rice and R. F. Boisvert, Solving Elliptic Problems with ELLPACK, Springer-Verlag, 1985.
[24] Y. Saad, Iterative Methods for Sparse Linear System. 2nd ed., SIAM, Philadelphia, (2003).
[25] E. SÃijli *Convergence of finite volume schemes for Poisson's equation on nonuniform meshes*, SIAM J. Numer. Anal., 28(5) (1993), pp. 1419–1430.
[26] J. C. Sun, *On approximation of Laplacian eigenproblem over a regular hexagon with zero boundary condition*, J. Comput. Math., 22(2) (2004), pp. 275–286.
[27] G. H. Zhou and S. R. Fulton, *Fourier analysis of multigrid methods on hexagonal grids*, SIAM J. Sci. Comput., 31(2) (2009), pp. 1518–1538.

https://doi.org/10.4208/nmtma.2017.m1527 Published online by Cambridge University Press